AD_____

Award Number: W81XWH-08-1-0240

TITLE: Multidisciplinary Biomarkers of Early Mammary Carcinogenesis

PRINCIPAL INVESTIGATOR: Julie Ostrander

CONTRACTING ORGANIZATION: Duke University
Durham, NC 27708

REPORT DATE: April 2011

TYPE OF REPORT: Annual Summary

PREPARED FOR: U.S. Army Medical Research and Materiel Command
Fort Detrick, Maryland 21702-5012

DISTRIBUTION STATEMENT: Approved for public release; distribution unlimited

REPORT DOCUMENTATION PAGE

Form Approved
OMB No. 0704-0188

1. REPORT DATE *(DD-MM-YYYY)*	2. REPORT TYPE	3. DATES COVERED *(From - To)*
01-04-2011	Annual Summary	15 MAR 2010 -14 MAR 2011

4. TITLE AND SUBTITLE
Multidisciplinary Biomarkers of Early Mammary Carcinogenesis

5a. CONTRACT NUMBER

5b. GRANT NUMBER
W81XWH-08-1-0240

5c. PROGRAM ELEMENT NUMBER

6. AUTHOR(S)
Julie Ostrander

E-Mail: hans1354@umn.edu

5d. PROJECT NUMBER

5e. TASK NUMBER

5f. WORK UNIT NUMBER

7. PERFORMING ORGANIZATION NAME(S) AND ADDRESS(ES)
Duke University
Durham, NC 27708

8. PERFORMING ORGANIZATION REPORT NUMBER

9. SPONSORING / MONITORING AGENCY NAME(S) AND ADDRESS(ES)
U.S. Army Medical Research and Materiel Command
Fort Detrick, Maryland 21702-5012

10. SPONSOR/MONITOR'S ACRONYM(S)

11. SPONSOR/MONITOR'S REPORT NUMBER(S)

12. DISTRIBUTION / AVAILABILITY STATEMENT
Approved for Public Release; Distribution Unlimited

13. SUPPLEMENTARY NOTES

14. ABSTRACT

The purpose of the proposed research is to develop novel optical technologies to identify high-risk premalignant changes in the breast. Our proposed research will first test specific optical parameters in breast cancer cell lines and models of early mammary carcinogenesis, and then develop methods to test the optical parameters in random periareolar fine needle aspirate (RPFNA) samples from women at high-risk for developing breast cancer. We have found that the optical redox ratio can 1) differentiate normal mammary epithelial cells from breast cancer cell lines, 2) differentiate ER(-) and ER(+) breast cancer cell lines and 3) monitor response to ER-targeted therapies. Our results suggest that the optical redox ratio will likely be able to differentiate normal mammary epithelial cells from premalignant changes. Further the optical redox ratio, in combination with other optical parameters, may be useful to monitor response to therapy, or predict response to therapy in patients with breast cancer and in small animal models.

15. SUBJECT TERMS
Optical spectroscopy, endogenous fluorophore, NADH, FAD, estrogen receptor (ER)

16. SECURITY CLASSIFICATION OF:			17. LIMITATION OF ABSTRACT	18. NUMBER OF PAGES	19a. NAME OF RESPONSIBLE PERSON
a. REPORT	b. ABSTRACT	c. THIS PAGE			USAMRMC
U	U	U	UU	36	19b. TELEPHONE NUMBER *(include area code)*

Table of Contents

INTRODUCTION

Progress in breast cancer prevention is currently limited by *1)* our inability to detect pre-invasive breast cancer and *2)* a lack of biological markers to risk-stratify mammary atypia. Optical Spectroscopy (auto fluorescence, absorption, and scattering) is a powerful experimental imaging technique that is currently being developed to exploit differences in the vascularity, hemoglobin oxygenation, fluorescent amino acids, metabolic proteins and structural proteins in normal and high-risk breast tissues. My mentor, *Dr. Nimmi Ramanujam* has shown that optical spectroscopy can differentiate metabolic differences between normal breast tissue from invasive breast cancer. The overall goal of our current research is to determine if Optical Spectroscopy can detect high-risk pre-invasive breast changes from normal breast tissue. We have taken a targeted approach, first specifically testing the optical redox ratio (NADH/FAD), which can be imaged by confocal microscopy. We have optimized the optical parameters in normal mammary epithelial cells and breast cancer cell lines and will move on to testing the optical redox ratio from epithelial cells obtained by Random Periareolar Fine Needle Aspiration (RPFNA). RPFNA is a research technique designed to prospectively sample breast cytology from asymptomatic high-risk women. My mentor, Dr. Victoria Seewaldt, has used RPFNA to test for pre-malignant cytological changes in over 250 high-risk women. In this multi-disciplinary postdoctoral fellowship, I will integrate the technology developed by my two mentors, to test whether the Optical Spectroscopy, can be used to improve the ability of RPFNA to predict short-term breast cancer risk.

Fluorescence microscopy is a useful tool to characterize the metabolic properties of normal and cancerous cells and tissue (1, 2). The primary oxidation-reduction (redox) reactions in cells to generate energy in the form of adenosine triphosphate (ATP) are the conversion of nicotinamide adenine dinucleotide (NAD^+) to its reduced form NAD(P)H (henceforth referred to as NADH), and the oxidation of flavin adenine dinucleotide (FAD) to $FADH_2$. A process known as oxidative phosphorylation. Both NADH and FAD are auto-fluorescent and have distinct excitation and emission maxima. The optical redox ratio can be determined by calculating the ratio of the measured fluorescence intensities of NADH and FAD (NADH/FAD) (3).

Alterations in cellular metabolism are an important hallmark of carcinogenesis (4). Cancer cell metabolism is often shifted from oxidative phosphorylation to aerobic glycolysis as the primary generator of cellular ATP. While the exact mechanisms for the switch to aerobic glycolysis and altered cellular metabolism are variable and complex (4, 5), it presents clear advantages for tumor growth. These advantages include resistance to fluctuations in the local oxygen concentration (6) and alterations in the tumor microenvironment that support tumor cell migration and invasion (7, 8). This shift, which gives rise to enhanced production of lactate in the presence of high oxygen, has long been known as the "Warburg effect" (9). In aerobic glycolysis, glucose is metabolized into two pyruvate molecules, which are then converted into lactate. This results in the production of two molecules of ATP and two NADH. During oxidative phosphorylation one molecule of glucose is converted to carbon dioxide and water, resulting in the production of 30 to 36 ATP molecules and the oxidation of 10 NADH molecules to NAD+. Thus, the switch from oxidative phosphorylation to aerobic glycolysis results in a net increase in NADH.

Estrogens and estrogen receptors (ERs) have been shown to play a role in numerous aspects of cellular metabolism in a number of organ systems, including the liver, pancreas, brain, muscle and breast (10, 11). Estrogens/ER have been shown to increase glucose transport and glycolysis (12-15). For example, estrogen exposure has been shown to increase expression of a number of glucose transporter (GLUT) proteins (12, 15, 16). Estrogen (but not the ER antagonist tamoxifen (Tam)) increased glucose uptake and lactate production in MCF-7 xenografts as measured by C^{13} nuclear magnetic resonance imaging (13). Additionally, estrogens/ER regulate gene expression of proteins involved in the citric acid cycle and oxidative phosphorylation (10). While not specifically studied in the breast, estrogen/ER has been shown to regulate citrate synthase, aconitase, and isocitrate dehydrogenase (17-20). Notably, isocitrate dehydrogense activity results in the reduction of NAD+ to NADH, which is expected to cause an increase in the optical redox ratio. Furthermore, ER has been shown to localize to the mitochondria in a variety of cell types (10) and it has been proposed that mitochondrial localization ER is important for the transcriptional regulation of numerous mitochondrial DNA encoded genes.

Previous studies have demonstrated that the optical redox ratio is statistically different between cancer and normal epithelial cells, with cancer cells exhibiting higher redox ratios (2, 3, 21, 22). For example, in a study comparing normal keratinocytes to HPV-transformed cells, the authors found that HPV-transformed cells had a higher overall intensity of NADH and lower overall intensity of FAD, which resulted in a statistically significant difference in the optical redox ratio (22). However, the optical redox ratio of NADH to FAD has not

been quantified for different biological subtypes of breast cancer, nor has its relationship to breast cancer ER status been assessed.

BODY

The first task outlined in the Statement of Work (SOW) was to "Acquire approval from the Department of Defense for research on samples from human subjects." This task has been accomplished and the proposed project has been approved by both the DoD and The University of Minnesota.

The second task was "To test UV-Visible fluorescence signatures in defined *in vitro* models of early mammary carcinogenesis." Based on our findings presented in the preliminary data section of the proposal (Figure 1), we first examined the optical redox ratio (NADH/FAD) on a broader panel of breast cancer cell lines. We quickly realized that in addition to cells segregating based on retinoid sensitivity, the optical redox ratio also differentiated cell lines based on expression of the estrogen receptor (ER). To date we have tested the optical redox ratio in a combined total of 11 normal mammary epithelial (2), ER(-) breast cancer (4) and ER(+) breast cancer (5) cell lines (Figure 2 and 3).

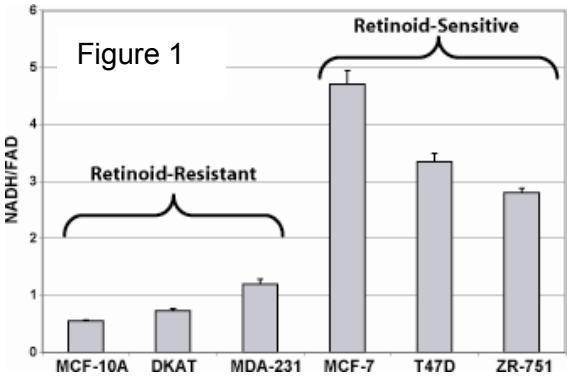

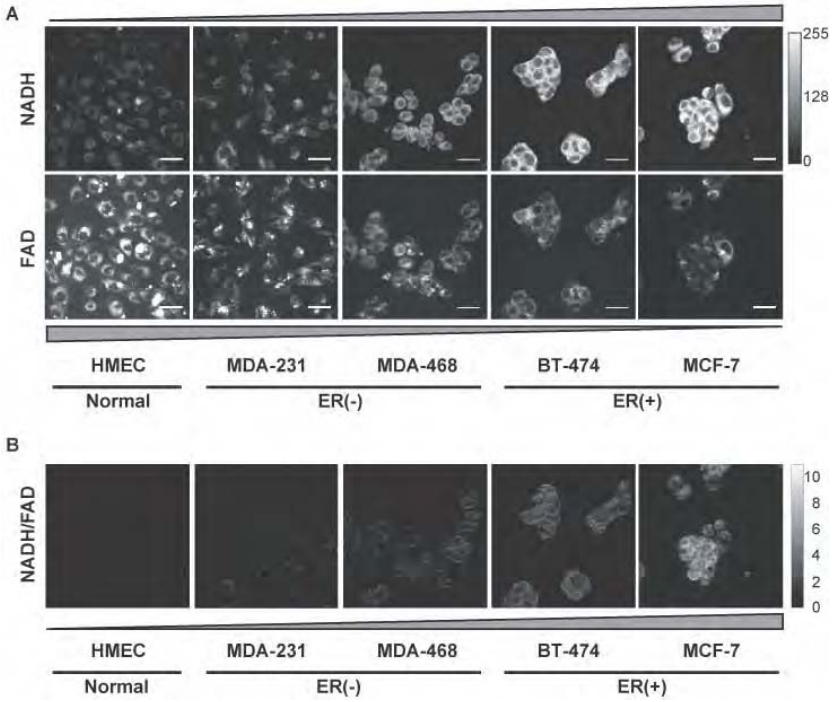

Figure 2. A. Representative NADH and FAD images from normal mammary epithelial cells (HMEC), ER(-) breast cancer cell lines (MDA-231 and MDA-468), and ER(+) breast cancer cell lines (BT-474 and MCF-7). Scale bar = 50 μM. **B.** Redox ratio images corresponding to representative images in (A), computed by dividing NADH images by FAD images pixelby-pixel. The color scale (shown at the right of the figure) was optimized for MCF7 cells and was kept constant for all images to allow direct visual comparison of redox ratio images across cell lines.

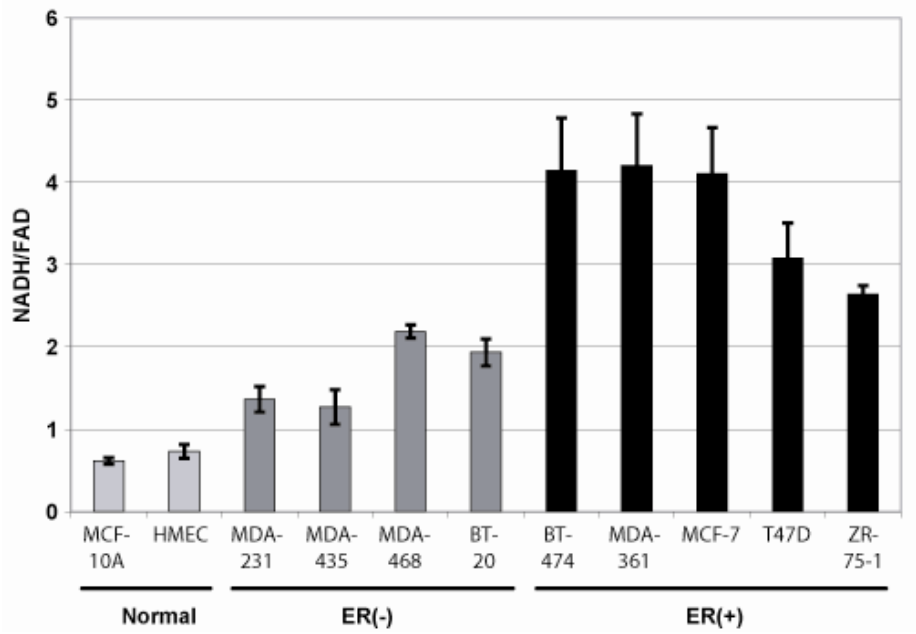

Figure 3. Optical Redox Ratio of breast cancer cell lines acquired using a Zeiss 410 laser scanning confocal microscope. NADH intensity images were obtained by excitation at 351 nm and collecting the fluorescence emission with a 400 nm LP filter. FAD intensity images were obtained by excitation at 488 nm and collecting the fluorescence emission with a 505 nm LP filter. At least 8 images were analyzed for each cell line. Every cell per image was analyzed separately. The optical redox ratio from all cells in an image was averaged, and the data from one image represented one data point (n = 1). Error bars represent standard error.

From this panel of cell lines we can make a number of conclusions. First, we found that all breast cancer cell lines have a statistically significant, by pairwise student's t-test, higher optical redox ratio compared to normal mammary epithelial cells. Second, if cell line data is grouped based on 1) normal mammary epithelial cells, 2) ER(-) breast cancer cells and 3) ER(+) breast cancer cells, all groups are statistically different from each other (student's t-test $p < 0.05$). This means that ER(+) cells have a higher redox ratio than ER(-) and normal mammary epithelial cells, and ER(-) cell lines have a higher redox ratio than normal mammary epithelial cells, but lower than ER(+) breast cancer cell lines (Figure 4).

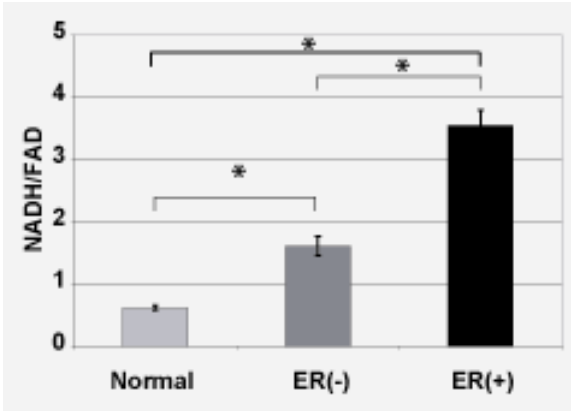

Figure 4. Data from cell lines shown in Figure 2 was combined based on ER receptor expression. Error bars represent standard error. Asterisk (*) $p < 0.0001$.

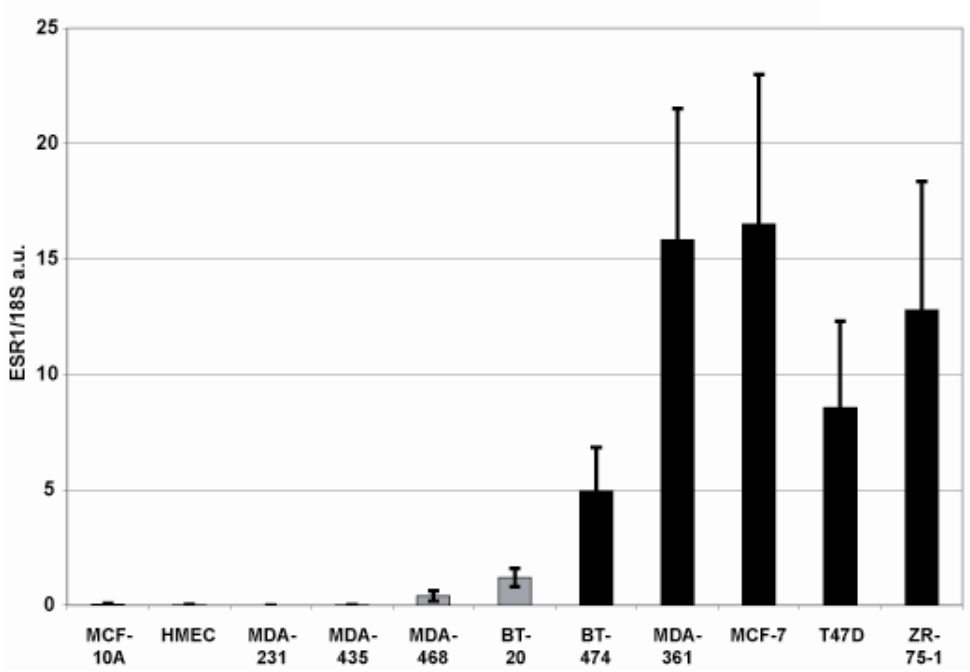

Figure 5. Total RNA was isolated from all cell lines and cDNA prepared. Quantitative real-time PCR (qRT-PCR) was then performed on the cDNA. All qRT-PCR reactions were performed in triplicate. ESR1 levels were normalized to qRT-PCR reactions for 18S rRNA. Figure 4 is the average of four separate experiments. Error bars represent standard deviation.

The cell line data suggests that expression of ER increases the optical redox ratio. To determine if ER expression correlates with the optical redox ratio, we performed quantitative real-time PCR on cDNA prepared from RNA isolated from each of the cell lines. As shown in Figure 4, all ER(+) cells express ESR1 at high levels (at least 4 fold higher than ER(-) cell lines). A Pearson correlation coefficient was calculated to determine the linear relationship between the optical redox ratio and ESR1 expression levels and found to be significant ($p = 0.0024$, $r = 0.81$), further suggesting that ER expression has an effect on the optical redox ratio.

We also tested for correlations between cellular growth rate and mitochondrial membrane potential, and the optical redox ratio. Cellular growth rate for each cell line was determined by MTT assay. Cells were plated at 1 x 10^4 cells/well in a 24-well plate. MTT assays were performed daily for seven days and the O.D. at 470nm was used as an estimate of cell number. Data was plotted over time, and fitted to an exponential curve ($R2>0.95$). The slope of the curve was plotted against the redox ratio as shown in Figure 6A. A spearman correlation test was performed to test for a linear correlation and found to be not statistically significant ($p = -0.70$, $r = 0.17$). Mitochondrial membrane potential (Ψm) was determined by incubated each cell line in JC-1. 5 x 10^5 cells were resuspended in MEMa with 1x JC-1 and incubated at 37°C, 5% CO2 for 15 minutes. Cells were washed in Assay Buffer and then resuspended in 300 mL of Assay Buffer. 100 mL was placed in 3 wells of a 96-well plate for each cell line. Red (mitochondrial) fluorescence was detected with excitation/emission wavelengths 525/ 580 – 640, while green (cytoplasmic) fluorescence was detected with excitation/emission wavelengths 490/510 – 570. $\Delta\Psi m$ was determined by mitochondrial/cytoplasmic fluorescence and then plotted against the redox ratio (Figure 6B). A spearman correlation test was performed to test for a linear correlation and found to be not statistically significant ($p = -0.36$, $r = 0.31$).

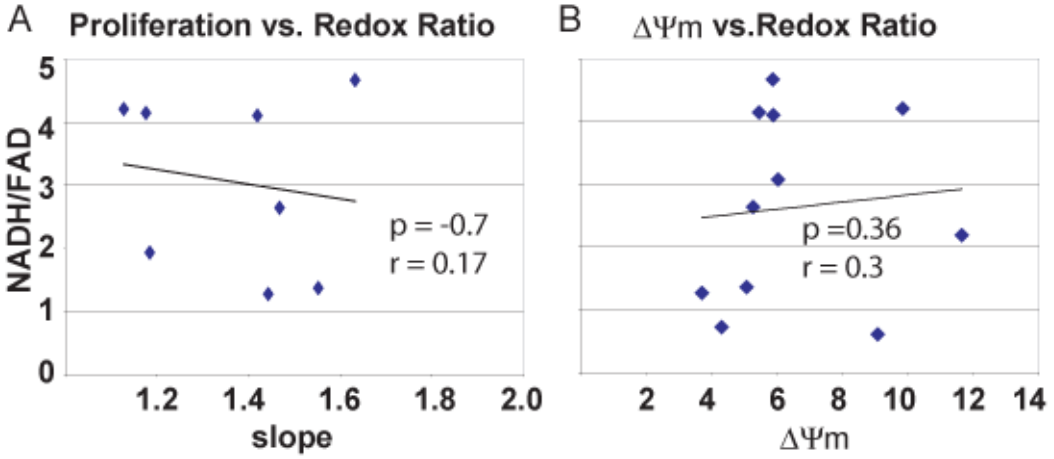

Figure 6. Cellular Proliferation (A) and mitochondrial membrane potential (B) of breast cancer cell lines plotted against the optical redox ratio.

Next, we performed a series of experiments to determine if inhibition of ER function has an effect on the optical redox ratio. First, ER function was inhibited with tamoxifen (Tam), an ER antagonist in the breast. Tam is known to promote cell cycle arrest and apoptosis in ER(+) breast cancer and is frequently prescribed to women with ER(+) breast cancer. Tam is also an effective chemoprevention drug for women at high-risk for developing breast cancer (23). ER(+) MCF-7 and T47D cells were treated with 2 μM tamoxifen (Tam) for 48 hours and the optical redox ratio was measured by confocal microscopy. We found that Tam significantly decreased the optical redox ratio of both MCF-7 and T47D breast cancer cells (Figure 7A). In a similar set of experiments we treated ER(+) MCF-7 cells and ER(-) MDA-231 cells with Tam and the pure antiestrogen ICI 182, 780 (ICI, Faslodex). As expected, Tam and ICI significantly reduced the optical redox ratio of MCF-7 cells, but had no effect on MDA-231 breast cancer cells (Figure 7B). We also acquired MCF-7 variant cell lines LCC2 and LCC9 from Robert Clarke at Georgetown University (24). LCC2 cells are Tam-resistant and ICI-sensitive, while the LCC9 cells are Tam- and ICI-resistant. Parental MCF-7, LCC2 and LCC9 cells were either left untreated or treated with ICI for 48 hours. ICI had a statistically significant effect on MCF-7 and LCC2 cells (student's t-test, $p < 0.05$), while the LCC9 cells were not effected by the ICI treatment (Figure 7C). Together, the data in Figure 6 suggest that ER antagonists reduce the optical redox ratio in ER(+) breast cancer cells, but not ER(-) or resistant cell lines.

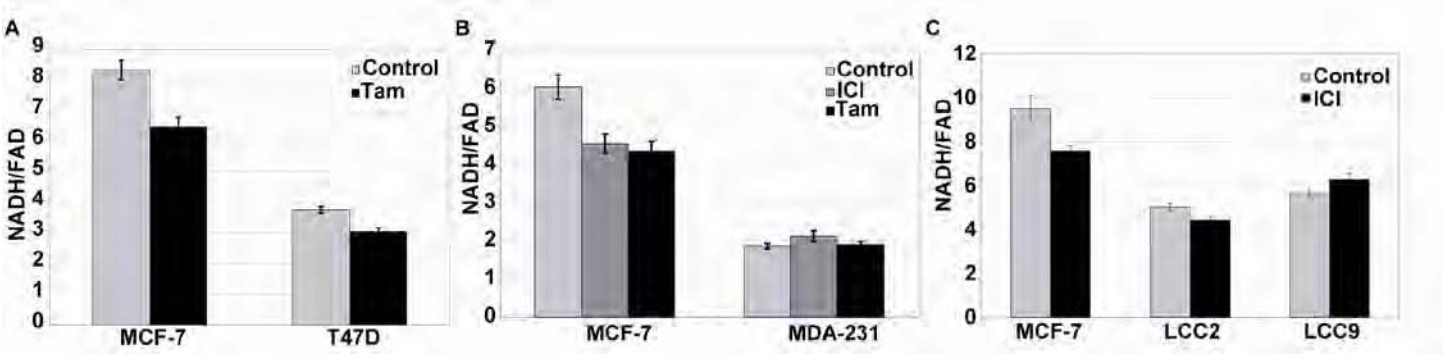

Figure 7. A, Optical redox ratio was measured by confocal microscopy from ER(+) MCF-7 and T47D cells that were treated with 2 μM tamoxifen (Tam) for 48 hours. **B,** Optical redox ratio was measured from control-, ICI-182,780- (ICI), and Tam-treated ER(+) MCF-7 and ER(-) MDA-231 cells. **C,** Optical redox ratio was measured from MCF-7 derived LCC2 (Tam-resistant, ICI-sensitive) and LCC9 (Tam-resistant, ICI-resistant), and MCF-7 cells treated with ICI for 48 hours.

The work described above was submitted for publication to Cancer Research in June of 2009. Both reviewers thought the manuscript was well written and contained "intriguing" and "novel" findings. Reviewer 1 recommended the manuscript for publication, but included a few minor comments to consider. These comments primarily focused on the speculative nature of the discussion and removal of Figure 3B. Reviewer 2 stated that the manuscript "is exciting and represents an important advance in the field of optical biomarkers", but to consider including one key experiment. Reviewer 2 requested that ER either be knocked down or overexpressed in ER+ or ER- cells, respectively.

In our response to the reviewer 2's comments we pointed out that we did in fact do a "knockdown" experiment when we treated ER+ cells with ICI 182,780. ICI 182,780 is an ER antagonist that targets ER for degradation. Reviewer 2 responded to our resubmission by acknowledging that "the authors correctly point out that the ICI experiment is the "knock-down" experiment.

In an effort to go beyond the reviewer's request, we also took a number of approaches to overexpress ER in ER- cells. This type of experiment is technically challenging, and this was acknowledged by the 2nd reviewer following the first submission. Both transient and stable expression approaches to express ER in ER- breast cancer cells. Because stable expression of ER would likely lead to growth suppression (25-28), we first tried to *transiently* transfect ER into ER- cells (MDA-435 and MDA-231). Using a variety of transfection reagents (i.e. Lipofectamine and Fugene) we were only able to achieve, at maximum, 20% transfection efficiency as determined by immunofluorescence microscopy (Figure 8A). A low transfection efficiency makes it difficult to 1) know which cells have been transfected during imaging, and 2) achieve statistically significant results and thus we did not pursue this further based on our findings.

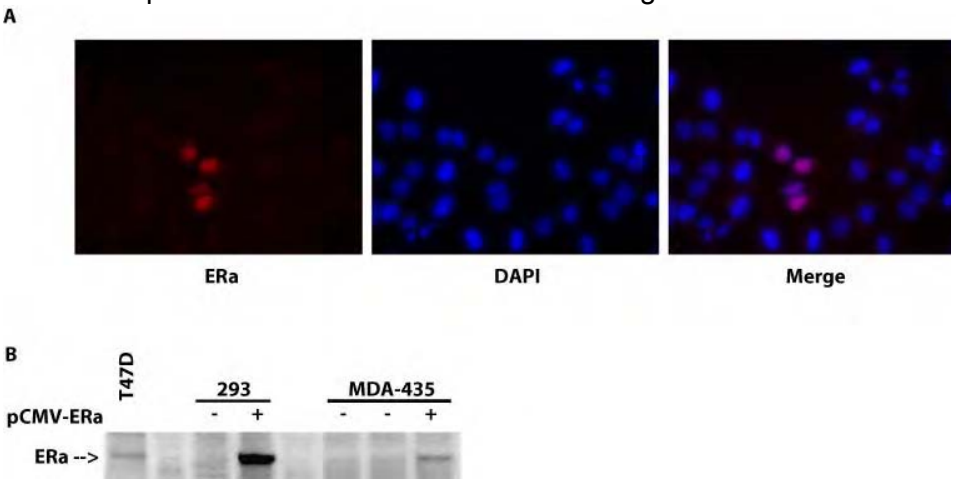

Figure 8. A. MDA-435 cells were transfected with pCMV-ERa using Fugene (Roche). 48 hours after transfection the cells were processed for immunofluorescence. The primary antibody antibody was a monoclonal for ER. Goat anti-mouse Alexafluor 594 was used as the secondary antibody and all slides were counterstained with DAPI. **B.** 293 and MDA-435 cells transfected with pCMV-ER and 48 hours following transfection cells were harvested for total protein. 30 ug of lysate was separated by SDS-PAGE and western blotting was performed for ER. T47D lysate was used as a positive control for ER expression.

Because transiently transfecting ER into ER- cells did not appear to be a viable way to overexpress ER, we attempted to *stably* express ER in ER- MDA-435 breast cancer cells and 293 human embryonic kidney cells. While we were able to observe ER expression by western blot 48 hours following transfection (Figure 7B), we did not obtain a pool of cells (from either cell line) that overexpressed ER following selection with G418, an antibiotic for which a resistance gene is encoded in the ER expression vector. This was likely due to the ability of ER to inhibit proliferation and/or induce cell death in cell lines that do not endogenously express ER (25-28).

This work was published in Cancer Research in June, 2010.

Following completion of the study described above, we had to optimize a new microscopy system because the system used in the previous study was decommissioned. While at Duke we tested three different systems, all available through the Light Microscopy Core Facility. The decommissioned Zeiss 410 confocal was converted to a 2-photon microscopy system. Since 2-photon microscopy should work well for imaging NADH and FAD our initial efforts focused on optimizing this system. Unfortunately, technical issues which required us to realign the laser between the NADH and FAD images and low signal intensity lead us to abandon this microscopy system. Next we tested the Leica SP5 confocal. While we were able to obtain nice images of NADH and FAD, we were not able to adequately separate the NADH and FAD signals (**Figure 9**). We did analyze the acquired images utilizing a number of different methods. The results of these analyses showed a similar trend, but were not as robust as what was published in our original study **(Figure 10)**. We believe that this was due to the excitation wavelength (405 nm) we were required to use with this microscopy system. In the published study we were exciting NADH at 351 nm. Next, we optimized the Zeiss upright 410 confocal system. This system was very similar to the original system, but not inverted and therefore we had to use a dipping objective to image the cells. This system was working fairly well and we were able to reproduce some of the cell line data from the published study.

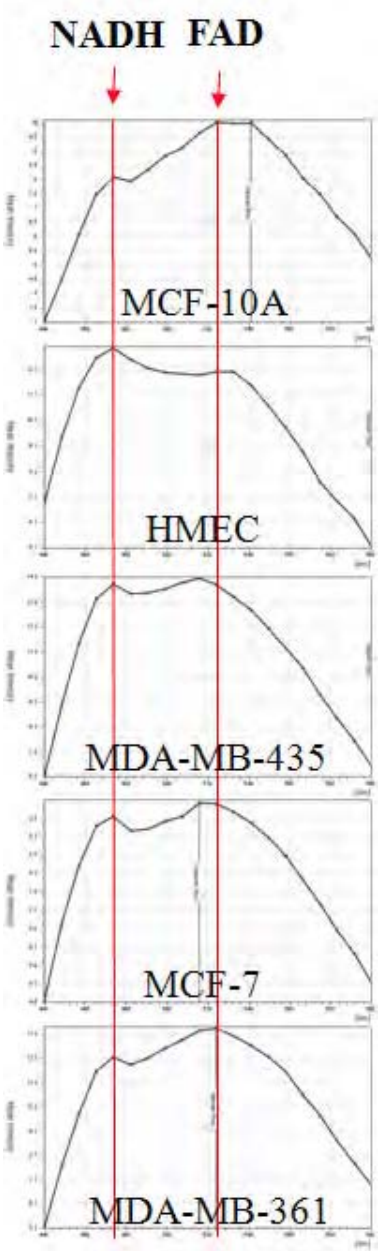

Figure 9. Spectral data obtained on the Leica SP5 confocal microscope from a 405 nm excitation

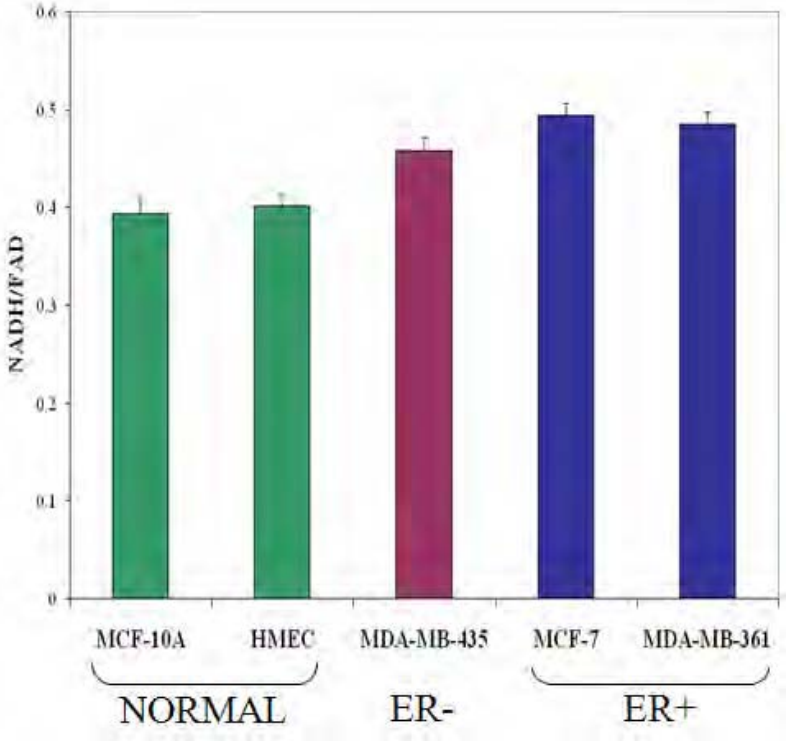

Figure 10. Optical redox ratio obtained using the SP5 Leica confocal microscope.

At this time, I accepted a position at the University of Minnesota. Through the Academic Health Center at the University of Minnesota I have access to the microscopy systems managed by the Biomedical Image Processing Lab (BIPL). Thus far we have tested two different systems. First, we tested the Zeiss Cell Observer Spinning Disk Confocal. We could clearly observe the NADH signal, but the FAD signal was too weak to continue using the microscopy system. Our initial tests with the Olympus FluoView 1000 IX2 Inverted Confocal indicate that this system should work well. We have acquired bright NADH and FAD images and see a dramatic difference in the optical redox ratio of HMEC and MCF-7 cell lines. We will further characterize this system and confirm that we can reproduce our published cell line data before moving on to more detailed experiments. As a side note, a colleague of mine at Vanderbilt University, Melissa Skala, is also using an Olympus FluoView 1000 IX2 Inverted Confocal microscopy system to image the optical redox ratio and she has reproduced our published work in a limited number of cell lines.

Since the submission of the last progress report, we have re-focused our efforts on the proposed statement of work. This included establishing models of early mammary carcinogenesis, via the knockdown/inhibition of RARβ and p53. We also focused our efforts on establishing a 3D rotary culture system, so we can examine the optical redox ratio, and other endogenous fluorphores, in intact mammary structures. All of these efforts are still in the preliminary stages in my new laboratory at the University of Minnesota.

KEY RESEARCH ACCOMPLISHMENTS

- We have shown that the optical redox ratio can clearly differentiate normal mammary epithelial cells from breast cancer cell lines.
- The optical redox ratio can differentiate ER(+) from ER(-) breast cancer cell lines.
- The optical redox ratio is modulated by ER expression and is reduced in the presence of ER antagonists.

REPORTABLE OUTCOMES

- Ostrander JH, et al. Optical Redox Ratio Differentiates Breast Cancer Cell Lines Based on Estrogen Receptor Status. Endocrine Society Meeting, San Francisco, CA; June 2008, Poster Presentation.
- Ostrander JH, et al. Optical Redox Ratio Differentiates Breast Cancer Cell Lines Based on Estrogen Receptor Status. DoD LINKs Meeting, Vienna, VA; February 2009, Poster Presentation.
- Millon SR, **Ostrander JH**, Yazdanfar S, Brown JQ, Bender JE, Rajeha A, and Ramanujam N. Preferential uptake of ALA-induced PpIX in breast cancer: A comprehensive study on six breast cell lines. *J Biomed Opt.* 2010 15(1):018002. PMID: 20210488 **(Appendix A)**
- Millon SR, **Ostrander JH**, Brown JQ, Raheja A, Seewaldt VL, Ramanujam N. Uptake of 2-NBDG as a method to monitor therapy response in breast cancer cell lines. Breast Cancer Res Treat. 2011 Feb;126(1):55-62. **(Appendix B)**
- **Ostrander JH,** McMahon CM, Lem S, Millon SR, Seewaldt VL, Ramanujam N. The Optical Redox Ratio Differentiates Breast Cancer Cell Lines Based on Receptor Status. Cancer Res. 2010 Jun 1;70(11):4759-66. **(Appendix C)**

The research described above was used as preliminary data for the submission of two grant applications in collaboration with Dr. Nimmi Ramanujam.

- DoD Era of Hope – BC087569. Harnessing the power of light to see and treat breast cancer. The goal of this proposal is to design and develop novel optical strategies to make current treatments for breast cancer faster and more effective, thereby reducing over- or under-treatment and the time and cost

burden associated with it. To achieve this, we will leverage optically detectable biomarkers that report on the physiological, metabolic, molecular and morphological state of the cancer, with novel technologies being developed by our team. This proposal was funded by the DoD.

- NIH R01 – AN:3146201. Multiparametric biomarker approach to asses tumor response to therapy. The goal of this R01 proposal is to develop a non-invasive, multi-parametric optical biomarker platform to dynamically characterize tumor hypoxia and angiogenesis in small animal models

CONCLUSION

Our results suggest that the optical redox ratio can 1) differentiate normal mammary epithelial cells from breast cancer cell lines, 2) differentiate ER(-) and ER(+) breast cancer cell lines and 3) monitor response to ER-targeted therapies. These studies provide further evidence that the optical redox ratio may identify premalignant changes from high-risk women. We will continue to develop models of mammary atypia and use our current methodologies to test our hypothesis in vitro. We are also developing new methodologies to test our hypothesis in samples from women at high-risk for developing breast cancer. Furthermore, these studies suggest that optical techniques may allow us to quickly determine if a woman is responding the chemoprevention therapies, such as tamoxifen.

While our results support the proposed research, there are also implications beyond the scope of the funded proposal. First, ER has proven to be a successful target of anti-tumor therapy in ER(+) breast tumors. However, resistance to anti-estrogen therapies is a serious clinical problem for the treatment of breast cancer. While ER expression is a good predictor of response to anti-estrogen therapies, not all ER(+) tumors respond to therapy and some develop resistance after initially responding to therapy. Therefore, the optical redox ratio may serve as an important biomarker to differentially identify ER(+) breast cancers and monitor response to anti-estrogen therapy with applications in drug discovery and screening as well as clinical assessment of response to anti-estrogen therapies.

Second, the optical redox ratio, in combination with additional optical parameters (total hemoglobin, hemoglobin saturation, and scattering), may have the power to assess the physiological, metabolic, morphological and molecular alterations in breast tissue in response to targeted and chemotherapies. To further investigate this possibility we (Dr. Ramanujam, Dr. Ostrander and others) recently submitted an Era of Hope proposal to the DoD BCRP.

Third, it is possible that Optical Spectroscopy and other molecular imaging modalities (such as optical coherence tomography (OCT)) when combined will have the power to quickly and efficiently monitor response to therapy and allow to further probe the molecular mechanisms associated with chemotherapy resistance. We have recently submitted an R01 proposal in which we propose to develop a non-invasive, multi-parametric optical biomarker platform to dynamically characterize tumor hypoxia and angiogenesis in small animal models. The system developed through these proposed studies will be a powerful tool for studies on mechanisms of tumor growth, resistance and response to therapy.

REFERENCES

1. Breslin TM, Xu F, Palmer GM, Zhu C, Gilchrist KW, Ramanujam N. Autofluorescence and diffuse reflectance properties of malignant and benign breast tissues. Annals of surgical oncology 2004;11(1):65-70.
2. Skala MC, Riching KM, Gendron-Fitzpatrick A*, et al.* In vivo multiphoton microscopy of NADH and FAD redox states, fluorescence lifetimes, and cellular morphology in precancerous epithelia. Proceedings of the National Academy of Sciences of the United States of America 2007;104(49):19494-9.
3. Chance B, Schoener B, Oshino R, Itshak F, Nakase Y. Oxidation-reduction ratio studies of mitochondria in freeze-trapped samples. NADH and flavoprotein fluorescence signals. The Journal of biological chemistry 1979;254(11):4764-71.
4. Kroemer G, Pouyssegur J. Tumor cell metabolism: cancer's Achilles' heel. Cancer cell 2008;13(6):472-82.
5. Brandon M, Baldi P, Wallace DC. Mitochondrial mutations in cancer. Oncogene 2006;25(34):4647-62.
6. Pouyssegur J, Dayan F, Mazure NM. Hypoxia signalling in cancer and approaches to enforce tumour regression. Nature 2006;441(7092):437-43.

7. Izumi H, Torigoe T, Ishiguchi H*, et al.* Cellular pH regulators: potentially promising molecular targets for cancer chemotherapy. Cancer treatment reviews 2003;29(6):541-9.
8. Walenta S, Wetterling M, Lehrke M*, et al.* High lactate levels predict likelihood of metastases, tumor recurrence, and restricted patient survival in human cervical cancers. Cancer research 2000;60(4):916-21.
9. Warburg O. On the origin of cancer cells. Science (New York, NY 1956;123(3191):309-14.
10. Chen JQ, Brown TR, Russo J. Regulation of energy metabolism pathways by estrogens and estrogenic chemicals and potential implications in obesity associated with increased exposure to endocrine disruptors. Biochimica et biophysica acta 2009;1793(7):1128-43.
11. Duckles SP, Krause DN, Stirone C, Procaccio V. Estrogen and mitochondria: a new paradigm for vascular protection? Molecular interventions 2006;6(1):26-35.
12. Cheng CM, Cohen M, Wang J, Bondy CA. Estrogen augments glucose transporter and IGF1 expression in primate cerebral cortex. Faseb J 2001;15(6):907-15.
13. Furman E, Rushkin E, Margalit R, Bendel P, Degani H. Tamoxifen induced changes in MCF7 human breast cancer: in vitro and in vivo studies using nuclear magnetic resonance spectroscopy and imaging. The Journal of steroid biochemistry and molecular biology 1992;43(1-3):189-95.
14. Kostanyan A, Nazaryan K. Rat brain glycolysis regulation by estradiol-17 beta. Biochimica et biophysica acta 1992;1133(3):301-6.
15. Welch RD, Gorski J. Regulation of glucose transporters by estradiol in the immature rat uterus. Endocrinology 1999;140(8):3602-8.
16. Macheda ML, Rogers S, Best JD. Molecular and cellular regulation of glucose transporter (GLUT) proteins in cancer. Journal of cellular physiology 2005;202(3):654-62.
17. Beckett T, Tchernof A, Toth MJ. Effect of ovariectomy and estradiol replacement on skeletal muscle enzyme activity in female rats. Metabolism: clinical and experimental 2002;51(11):1397-401.
18. Pastorelli R, Carpi D, Airoldi L*, et al.* Proteome analysis for the identification of in vivo estrogen-regulated proteins in bone. Proteomics 2005;5(18):4936-45.
19. Stirone C, Duckles SP, Krause DN, Procaccio V. Estrogen increases mitochondrial efficiency and reduces oxidative stress in cerebral blood vessels. Molecular pharmacology 2005;68(4):959-65.
20. Yadav RN. Isocitrate dehydrogenase activity and its regulation by estradiol in tissues of rats of various ages. Cell biochemistry and function 1988;6(3):197-202.
21. Kirkpatrick ND, Zou C, Brewer MA, Brands WR, Drezek RA, Utzinger U. Endogenous fluorescence spectroscopy of cell suspensions for chemopreventive drug monitoring. Photochemistry and photobiology 2005;81(1):125-34.
22. Mujat C, Greiner C, Baldwin A*, et al.* Endogenous optical biomarkers of normal and human papillomavirus immortalized epithelial cells. International journal of cancer 2008;122(2):363-71.
23. Fisher B, Costantino JP, Wickerham DL*, et al.* Tamoxifen for prevention of breast cancer: report of the National Surgical Adjuvant Breast and Bowel Project P-1 Study. Journal of the National Cancer Institute 1998;90(18):1371-88.
24. Brunner N, Boysen B, Jirus S*, et al.* MCF7/LCC9: an antiestrogen-resistant MCF-7 variant in which acquired resistance to the steroidal antiestrogen ICI 182,780 confers an early cross-resistance to the nonsteroidal antiestrogen tamoxifen. Cancer research 1997;57(16):3486-93.
25. Ali SH, O'Donnell AL, Balu D*, et al.* Estrogen receptor-alpha in the inhibition of cancer growth and angiogenesis. Cancer research 2000;60(24):7094-8.
26. Ali SH, O'Donnell AL, Mohamed S, Mousa S, Dandona P. Stable over-expression of estrogen receptor-alpha in ECV304 cells inhibits proliferation and levels of secreted endothelin-1 and vascular endothelial growth factor. Molecular and cellular endocrinology 1999;152(1-2):1-9.
27. Jiang SY, Jordan VC. Growth regulation of estrogen receptor-negative breast cancer cells transfected with complementary DNAs for estrogen receptor. Journal of the National Cancer Institute 1992;84(8):580-91.
28. Kushner PJ, Hort E, Shine J, Baxter JD, Greene GL. Construction of cell lines that express high levels of the human estrogen receptor and are killed by estrogens. Molecular endocrinology (Baltimore, Md 1990;4(10):1465-73.

Preferential accumulation of 5-aminolevulinic acid-induced protoporphyrin IX in breast cancer: a comprehensive study on six breast cell lines with varying phenotypes

Stacy R. Millon
Duke University
Department of Biomedical Engineering
3000 Science Drive Hudson Hall
Box 90281
Durham, North Carolina 27708-0281

Julie H. Ostrander
Duke University
Department of Medicine
Box 2628 Medical Center
Durham, North Carolina 27710

Siavash Yazdanfar
General Electric Global Research Center
1 Research Circle
Niskayuna, New York 12309

J. Quincy Brown
Janelle E. Bender
Anita Rajeha
Nirmala Ramanujam
Duke University
Department of Biomedical Engineering
3000 Science Drive Hudson Hall
Box 90281
Durham, North Carolina 27708-0281

Abstract. We describe the potential of 5-aminolevulinic acid (ALA)–induced protoporphyrin IX (PpIX) fluorescence as a source of contrast for margin detection in commonly diagnosed breast cancer subtypes. Fluorescence intensity of PpIX in untreated and ALA-treated normal mammary epithelial and breast cancer cell lines of varying estrogen receptor expression were quantitatively imaged with confocal microscopy. Percentage change in fluorescence intensity integrated over 610–700 nm (attributed to PpIX) of posttreated compared to pretreated cells showed statistically significant differences between four breast cancer and two normal mammary epithelial cell lines. However, a direct comparison of post-treatment PpIX fluorescence intensities showed no differences between breast cancer and normal mammary epithelial cell lines due to confounding effects by endogenous fluorescence from flavin adenine dinucleotide (FAD). Clinically, it is impractical to obtain pre- and post-treatment images. Thus, spectral imaging was demonstrated as a means to remove the effects of endogenous FAD fluorescence allowing for discrimination between post-treatment PpIX fluorescence of four breast cancer and two normal mammary epithelial cell lines. Fluorescence spectral imaging of ALA-treated breast cancer cells showed preferential PpIX accumulation regardless of malignant phenotype and suggests a useful contrast mechanism for discrimination of residual cancer at the surface of breast tumor margins.
[DOI: 10.1117/1.3302811]

Keywords: 5-aminolevulinic acid; breast cells; confocal microscopy; fluorescence intensity; protoporphyrin IX; spectroscopy.

Paper 09142RR received Apr. 13, 2009; revised manuscript received Oct. 26, 2009; accepted for publication Nov. 30, 2009; published online Feb. 18, 2010.

1 Introduction

Women with early stage breast cancer are eligible for breast conserving surgery (BCS). The goal of BCS is to remove the entire tumor while minimizing removal of surrounding normal tissue. The commonly accepted pathologic criterion for a negative margin is a 2-mm rim of malignancy-free tissue.[1] There are no widely adopted intraoperative tools to assess tumor margins, and all decisions are made postoperatively by a pathologist. If the margin is positive, then a secondary surgical procedure is performed to excise additional tissue and prevent local recurrence of cancer. On average, four out of ten women undergoing BCS return for a reexcision surgery.[2–10] Thus, a critical need exists for new tools that can be used intraoperatively to determine if a tumor margin is positive or negative at the time of the first surgery.

Optical techniques that exploit exogenous contrast agents, such as antibody-conjugated gold nanoparticles[11,12] or fluorescence molecules,[13,14] are currently being investigated to enhance a surgeon's ability to identify malignancy, with one possible use being intraoperative margin assessment. A contrast agent such as 5-aminolevulinic acid (ALA) is one potential candidate for margin assessment. ALA has been extensively tested in cells, animal models, and humans[15–41] and is widely used today for detection and treatment of malignancy. Addition of exogenous ALA causes a preferential accumulation of protoporphyrin IX (PpIX) in cancerous cells when compared to normal cells.[15–31,33–36,39,40] PpIX is naturally produced by all nucleated cells during the heme cycle and meticulously controlled to prevent its natural accumulation.[37] This negative feedback system is thought to be modified in cancerous tissues due to (*i*) enzymatic defects that lead to an increase in protoporphyrinogen IX oxidase and/or (*ii*) reduced activity of ferrochelatase.[35]

Address all correspondence to: Stacy R. Millon, Duke University, Department of Biomedical Engineering, 3000 Science Drive Hudson Hall, Box 90281, Durham, North Carolina 27708-0281; Tel: 919-660-8473; Fax: 919-684-4488; E-mail stacy.millon@duke.edu

1083-3668/2010/15(1)/018002/8/$25.00 © 2010 SPIE

ALA and its derivatives have shown great potential to photodynamically detect and treat cancer in a wide variety of organs and applications. Clinical approval of ALA derivatives has been granted in the European Union for photodynamic diagnosis of cancer of the bladder, brain, and skin, but has only been approved for use on skin by the Food and Drug Administration in the United States.[22] Preferential accumulation of PpIX in tumor cells, specifically residual glioma cells within the excision cavity,[37,42] followed by photodynamic therapy of those cells, demonstrates the potential of ALA for use in a "see-and-treat" paradigm in breast cancer.[22,37,43] ALA-induced PpIX has been shown to have a higher accumulation in cancerous breast cells as compared to prostate, ovarian, and brain cancer cell lines, which implies higher contrast and effective visualization of cancerous cells.[18,30] ALA-induced phototherapy in breast cancer cells (MDA-MB-231) has demonstrated high photoefficiency, further demonstrating the potential for the see-and-treat paradigm within breast tissue.[43]

Previous studies illustrate that ALA-induced PpIX has the capability to differentially detect breast cancer in multiple biological model systems.[18,20,29,30,36,40] Fluorescence quantification of PpIX in breast cancer cell lysates treated with ALA was higher as compared to patient-matched normal cell lysates treated with ALA in explanted cell cultures from five breast cancer patients.[28] Studies on an *in vivo* animal model have shown that ALA-induced fluorescence can be used to enhance early detection of neoplastic and metastatic tissue from normal tissue.[36] Transgenic mice with induced ductal carcinoma *in situ*, the earliest form of breast cancer, were shown to have an increase in 635 nm fluorescence (attributed to PpIX) in cancerous tissues over the surrounding normal tissues, after tail-vein injection of ALA 60–75 min prior to imaging.[36] In a clinical study, ALA-induced PpIX fluorescence was significantly greater in 13 *ex vivo* primary breast tumors relative to surrounding normal tissue.[24] Metastatic axillary and sentinel lymph node tissues imaged *ex vivo* also showed an increase in mean PpIX fluorescence as compared to nonmetastatic lymph nodes in seven breast cancer patients.[15]

The clinical applicability of ALA-induced PpIX has been demonstrated by the early clinical work of Ladner et al.,[24] but before diagnosis of breast cancer with ALA is widely accepted, more fundamental cellular, animal, and clinical studies will be required to characterize the effects of breast cancer subtype on uptake and contrast. Breast cancer is highly heterogeneous and has been shown to exhibit large variations in characteristics that may potentially affect metabolism of contrast agents, such as ALA-induced PpIX.

The goal of the study reported here was to evaluate ALA-induced PpIX fluorescence of a variety of breast cancer cell lines of varying phenotypes that are most commonly seen clinically[44] and compare their ALA-induced PpIX fluorescence to those of normal mammary epithelial cells.[23] Specifically, confocal microscopy at 405 nm excitation was utilized to image ALA-induced PpIX fluorescence in a panel of six different breast cell lines—two normal, two estrogen receptor negative (ER−), and two ER positive (ER+)—before and after treatment with ALA. This is the first study to establish the sources of contrast in different breast cancer and normal epithelial cells after application of PpIX. Confocal microscopy is an ideal modality for cell studies due to its high-resolution capabilities. Imaging of ALA-induced PpIX fluorescence for intraoperative margin assessment will likely need full-field imaging techniques, with a larger field of view and higher speed than confocal fluorescence imaging.

2 Methods and Materials

2.1 *Cell Culture*

Six breast cell lines were used in this study; two were normal mammary epithelial cells [MCF10A and human mammary epithelial cells (HMEC)] and four were breast cancer (MDA-MB-231, MDA-MB-361, MDA-MB-435, and MCF7). All cell lines, except for HMEC, were obtained from the American Type Culture collection (Manassas, Virginia). HMEC primary cells were obtained from Lonza (Basel, Switzerland) and infected with a retrovirus encoding human telomerase reverse transcriptase for immortalization. All cells remained free of contaminants and were propagated by adherent culture according to established protocols.[44] All breast cancer cell lines were cultured in α-MEM (Minimum Essential Media, Gibco, Carlsbad, California) supplemented with 6% fetal bovine serum, 1% hepes, 1% nonessential amino acids, 1% of 100 mM sodium pyruvate, 10 μg/mL insulin, 10 μg/mL hydrocortisone, and 5 μg/mL epidermal grown factor (EGF). All normal mammary epithelial cell lines were cultured in mammary epithelial basal media (MEBM) (Lonza, Basel, Switzerland) with 0.4% bovine pituitary extract, 0.01% hydrocortisone, insulin, and human EGF. Plated cells were incubated at 5% CO_2 and cultured every 3–4 days. Cells were double washed in 3 mL of phosphate buffer saline and detached from flasks with 0.25% trypsin before centrifugation.

After 3 min of centrifugation at 120 relative centrifugal force (rcf), a standard hemocytometer was used to count the number of cells per milliliter. Approximately 200,000 cells were plated on a 35-mm coverslip dish (Mat-Tek, Ashland, Massachusetts) to be tested.

2.2 *Confocal Microscope and Imaging Parameters*

All confocal images were collected at the Duke University Light Microscopy Core Facility on a Leica SP5 laser scanning confocal microscope (Wetzlar, Germany). All cells were imaged in a temperature-controlled (37 °C) live cell chamber. A 405-nm diode laser source with a mean power of 2.4 mW at the sample plane and scanning rate of 400 Hz was coupled to an inverted Leica DM16000CS microscope with a 40X oil-immersion objective (Leica Plan NeoFluor, NA=1.25). The imaging field of view was 242×242 μm with 512×512 pixels per image. An acousto-optic beamsplitter (AOBS) served as a dichroic mirror to allow the 405-nm excitation light to reach the sample and to allow selection of emission wavelengths. Cooled photomultiplier tubes (PMTs) were used to measure fluorescence through a 121-μm pinhole in a confocal arrangement with a theoretical axial resolution of 2 μm.

The emission bandpass for integrated fluorescence intensity measurements was set to 610–700 nm, which was chosen from preliminary spectroscopy data on cells that showed a fluorescence peak at 630 nm, corresponding to PpIX, as pub-

Table 1 Experimental sample size for confocal microscopy.

	Sample size definition		No. Images/ plate	No. plates	Total No. of samples
Integrated fluorescence intensity	Treated	1 Sample=Average intensity of all cells per image	6	2	12 per cell line
	Untreated	1 Sample=Average intensity of all cells per image	6	2	12 per cell line
Spectrally resolved fluorescence	Treated	1 Sample=3 spectra averaged from a cluster of cells (3–5 cells) per image	6	2	12 per cell line
	Untreated	1 Sample=3 spectra averaged from a cluster of cells (3–5 cells) per image	1	1	1 per cell line

lished in the literature.[42] Images were taken at two separate fields of view and line averaged (16X per line) for improved image quality. Each fluorescence intensity image was acquired in ~20 s per image (1/400 per second 16 averages per line×512 lines per image). Spectrally resolved fluorescence images at 405 nm excitation were collected at each of 34 emission wavelengths between 420 and 750 nm with a line average of 1. The AOBS had a collection bandwidth of 20 nm. A prism with a sliding mirror placed in the optical path prior to the PMT was scanned every 10 nm to ensure Nyquist sampling was fulfilled across all wavelengths. Total acquisition time was 43.5 s for all wavelengths in each spectral image (1/400 per second 1 average per line×512 lines ×34 wavelengths per spectral image). Leica LAS AF 1.8.2 software (Wetzlar, Germany) was used for data acquisition. All images (intensity and spectral) were acquired with a gain of 1200 V, offset 0.7% and zoom of 1.6.

Prior to imaging, a calibration intensity image of standard fluorescent beads was obtained (FocalCheck Fluorescence Microscope Test Slide No. 2, Invitrogen, Carlsbad, California) to correct for daily variations in microscope throughput. The mean fluorescence intensity over all experiments was 208±5 units. Integrated fluorescence intensity images were normalized by dividing the measured intensity by the intensity of the calibration standard measured on the same day.

2.3 *Cell Imaging*

Twenty-four hours after plating, the original cell media was removed from the culture dish, and cell lines were treated either with 500 μg/mL of ALA in standard cell media or standard media alone and incubated for 2 h prior to imaging. Because ALA is not fluorescent, it was not removed before imaging. The concentration of ALA (data not shown) was chosen experimentally. At 500 μg/mL of ALA, no phototoxic effects were seen in any cell line tested for this paper. Cell viability was verified by a trypan blue exclusion assay as determined by a previously tested protocol.[45] Viable cell concentration was then determined by counting the ratio of cells that were still viable (unstained) to all cells, and 89%±6% of ALA-treated and 85%±8% of untreated cells were found to be viable. Finally, 500 μg/mL of ALA was found to be within the range of concentrations used in previous cell culture studies.[18,40]

To determine the optimal time to measure the fluorescence of PpIX (data not shown), a subset of cells [normal mammary epithelial MCF10A, MDA-MB-435 (ER−), and MCF7 (ER+)] was tested. The fluorescence intensity increased linearly from 0 to 6 h post-ALA treatment, as seen in previous studies,[40] and therefore, the peak intensity window was assumed to be >6 h post-ALA treatment for all cell lines. The 2-h time point was chosen because it is clinically practical and showed distinct differences between normal mammary epithelial and breast cancer cell lines (see Sec. 3).

The sample size for each cell line included 12 treated and seven untreated plates. Fluorescence intensity images were obtained from six of the treated and six of the untreated plates. Confocal spectral imaging was completed on six additional treated plates and a single untreated plate for each cell line. Sample size calculations for imaging of integrated fluorescence and confocal spectral imaging are summarized in Table 1.

2.4 *Analysis of Integrated Fluorescence Intensity Images*

Integrated fluorescence intensity images were analyzed using NIH ImageJ software. Integrated fluorescence intensity for each breast cell line was determined by manually segmenting each cell in the image and then computing the average fluorescence intensity. Background intensity was subtracted, and the resulting data normalized by the fluorescence of the calibration was standard. The background was defined as an area

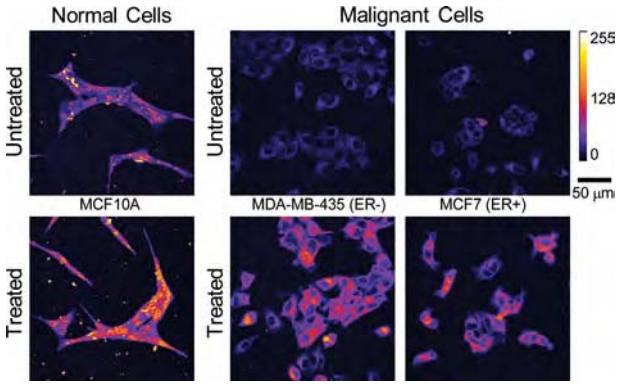

Fig. 1 Representative confocal integrated fluorescence intensity images (uncalibrated) of normal mammary epithelial (Normal) and breast cancer (Malignant) cells treated with ALA for 2 h. Excitation was at 405 nm, and emission was collected between 610 and 700 nm.

without cells that was approximately equivalent to the size of an entire cell (2000–5000 pixels, depending on the cell line). Fluorescence intensity values for all cells within each image were then averaged to represent one sample (each image had approximately 10–50 cells within a field of view, depending on the cell line). A total of $n=12$ fields of view (two images per sample) were imaged, from which the average integrated fluorescence intensity per cell line was derived for both treated and untreated cells.

2.5 *Analysis of Spectrally Resolved Fluorescence Images*

For spectrally resolved fluorescence images, a spectrum was calculated by the Leica software from an area of 3–5 adjacent cells (6000–15,000 pixels, depending on the cell line). Three groups of adjacent cells were manually segmented, and all spectra were averaged to obtain a single spectrum (three per image). A background spectrum was obtained from a cell-free region in each image (2000–90,000 pixels, depending on the cell-line growth pattern) and subtracted from each of the three spectra. These three spectra were imported into MATLAB (Mathworks, Inc., Natick, Massachusetts) to calculate Fractional PpIX contribution (FPC). (See Section 3 for further discussion of this calculation). The three FPC values from each image were averaged to obtain a single FPC per image. A total of $n=12$ FPCs (two images per sample) was calculated for all six treated cell plates, from which the average FPC for the cell line was calculated.

2.6 *Statistics*

All statistics were computed with JMP (SAS, Cary, North Carolina) software. ANOVAs and t-tests were completed with a Tukey–Kramer correction for multiple comparisons to determine statistical significance. Exact two-sided p-values were computed, and all $p<0.05$ were considered significant. All calculated correlations are reported with a Pearson coefficient.

3 Results

3.1 *Integrated Fluorescence Intensity Images*

Figure 1 shows representative integrated fluorescence intensity images of untreated and treated cell lines with different ER phenotypes. The untreated normal mammary epithelial cell line image has much higher pretreatment endogenous fluorescence than either breast cancer cell line, which is likely due to the endogenous fluorophore, FAD. Bright specks outside of the cells in the normal column are cellular debris caused by plating on untreated glass and were not included in subsequent analyses. Untreated ER− and ER+ breast cancer cell lines qualitatively show similar distributions of endogenous fluorescence, which is diffusely distributed throughout the breast cancer cells prior to treatment and a few areas of high intensity around the nucleus. All cells showed an increase in PpIX fluorescence after 2 h of ALA treatment, as seen in the "Treated" row in Fig. 1. The normal mammary epithelial cell line shows bright points of PpIX fluorescence within an even distribution of cellular fluorescence. Breast cancer cell lines show brighter fluorescence in the perinuclear cytoplasm, and although the edges of the cells are clearly visible in the post-treatment images, the edges are not as intense. PpIX fluorescence is only in the cellular cytoplasm (as opposed to the nucleus) in all cell lines.

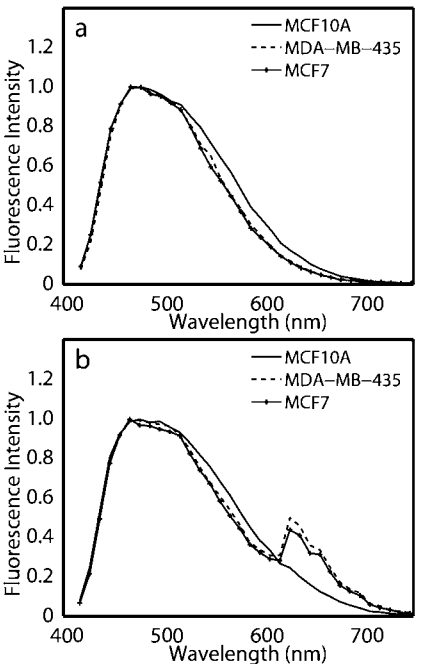

Fig. 2 Representative normalized fluorescence spectra at 405-nm excitation of (a) untreated cells and (b) ALA-treated cells. Spectra were normalized to the peak intensity.

3.2 *Cellular Fluorescence Spectra*

Figure 2 shows normalized representative fluorescence spectra from one untreated [Fig. 2(a)] and one ALA-treated plate [Fig. 2(b)] of normal mammary epithelial, ER−, and ER+ cell lines at 405 nm excitation. Excitation at 405 nm is expected to elicit fluorescence from FAD and PpIX.[46] Normalized representative spectra in Fig. 2 show a single broad emission, which is due to FAD, and spectra from treated cells show an additional distinct ALA-induced PpIX emission peak at 630 nm with a shoulder at 700 nm [Fig. 2(b)], similar to that observed by others.[46] It should be noted that the tail of the

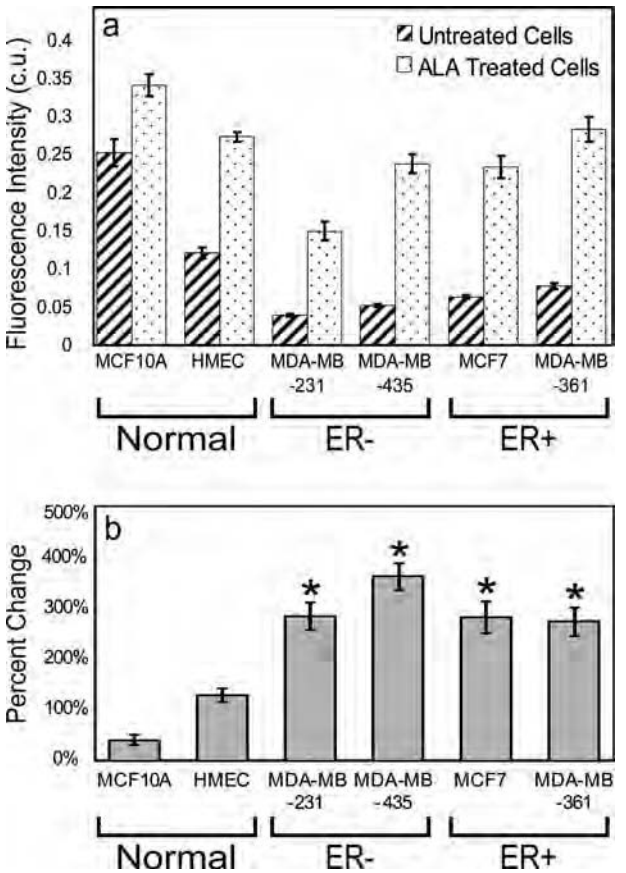

Fig. 3 Average and standard error of the (a) calibrated integrated fluorescence intensity (c.u.) per cell line ($n=12$) and (b) percentage change in integrated fluorescence intensity of treated compared to the untreated controls ($n=12$). Asterisks denote that each ALA-treated breast cancer cell line has a statistically higher percentage change in integrated fluorescence compared to ALA-treated normal mammary epithelial cell lines (Normal) ($p<0.05$).

FAD fluorescence spectrum overlaps with the PpIX fluorescence between 610 and 700 nm [Fig. 2(b)], and therefore, it is assumed to contribute to integrated fluorescence intensity images collected over a bandpass of 610–700 nm.

3.3 *Quantitative Integrated Fluorescence Intensity Measurements*

In Fig. 3, the six cell lines were grouped in pairs by ER expression (normal mammary epithelial, malignant ER−, and malignant ER+). All cell lines exhibited significantly greater fluorescence intensity following treatment ($p<0.05$). The normal mammary epithelial cell lines (MCF10A and HMEC) untreated fluorescence intensity was significantly greater than all untreated breast cancer (MDA-MB-231, MDA-MB-435, MCF7, and MDA-MB-361) cell lines [Fig. 3(a), $p<0.01$]. Calibrated fluorescence intensity of the ALA-treated HMEC cell line was significantly greater than the treated MDA-MB-231 breast cancer cell line, but not significantly different compared to the other ALA-treated breast cancer cell lines. Figure 3(b) shows that the percentage change in PpIX fluorescence intensity following treatment was significantly greater in all breast cancer cell lines as compared to both normal mammary epithelial cell lines by at least 150% [Fig. 3(b), $p<0.05$]. No significant differences in the percent change of fluorescence intensity were observed between or within the ER− and ER+ breast cancer cell lines.

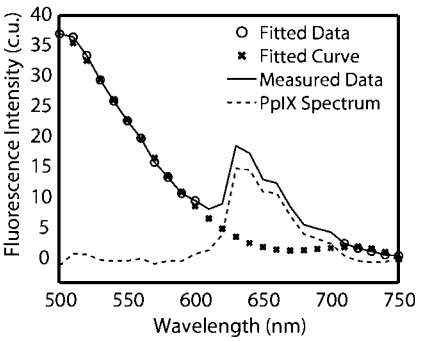

Fig. 4 Representative spectral data (—), spectral data used in fit (○), polynomial fit (×), and the resulting PpIX spectrum (--).

3.4 *Quantitative analysis of the fluorescence spectral data*

Although the breast cancer cells demonstrated a significant percentage increase in fluorescence following ALA treatment, it may be clinically impractical to obtain a pretreatment measurement. Post-treatment intensity measurements alone were not useful in discriminating normal mammary epithelial cell lines from breast cancer due to cell-to-cell variability in endogenous FAD fluorescence. A method for differentiating between normal mammary epithelial and breast cancer cells using only post-treatment measurements would be desirable. Fluorescence spectral images that capture both FAD and PpIX fluorescence have the potential to directly address this problem as presented below.

The contribution of FAD fluorescence to the PpIX fluorescence was quantified and removed as shown in Fig. 4. First, the spectrum between 520–600 nm and 700–750 nm (○) was fit with a fourth-order polynomial to approximate an untreated spectrum (×). All polynomials were shown to have a goodness-of-fit coefficient (r) of 0.93. The fitted curve (×) was then subtracted from the measured data (—), which resulted in an FAD-subtracted PpIX spectrum (--). The area under the curve of the resulting PpIX spectrum was calculated over 610–700 nm and represents integrated PpIX fluorescence intensity. The area under the curve of the fitted FAD spectrum was calculated to represent the integrated baseline FAD fluorescence intensity. Then, FPC was calculated as the ratio of integrated PpIX and FAD fluorescence intensities.

Figure 5 shows the FPC for each cell line. All breast cancer cell lines have a significantly higher FPC than normal mammary epithelial cell lines. It is not surprising to note that the FPC and percentage change in fluorescence intensity, (Figs. 3 and 5), are significantly and positively correlated (Pearson coefficient=0.92, $p<0.05$). No differences in FPC were observed between ER+ and ER− cell lines. Therefore, it can be said that PpIX fluorescence is preferentially accumulated in all breast cancer cells studied here, regardless of ER expression.

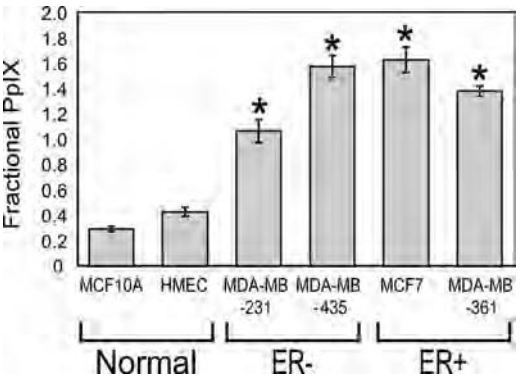

Fig. 5 Average and standard error of the FPC. Asterisks denote that the FPC of each breast cancer cell line is significantly higher than those of both normal mammary epithelial cell lines ($p<0.05$).

4 Discussion

This study demonstrates the ability of ALA-induced PpIX to discriminate breast cancer cell lines from normal mammary epithelial cells. Breast cancer cell lines used in this study comprised a variety of phenotypes, including ER− and ER+ (ER is expressed in ~60% of all breast cancers).[47] The research showed that fluorescence of ALA-treated cells (two normal mammary epithelial and four breast cancer cell lines) was significantly greater than the equivalent untreated cell lines. Also, breast cancer cell lines could be easily discriminated from normal mammary epithelial cell lines by determining the percentage change in fluorescence intensity after PpIX treatment. However, the high endogenous FAD fluorescence present in untreated normal mammary epithelial cells resulted in overall greater post-treatment fluorescence in normal mammary epithelial cells compared to breast cancer cells and demonstrated the need for a method to account for the cell-to-cell variability in FAD fluorescence in the absence of pretreatment images. Spectroscopy provided a means of separating endogenous fluorescence contribution from ALA-induced PpIX fluorescence and enabled discrimination of normal mammary epithelial and breast cancer cells based on a single post-treatment measurement.

Ratiometric methods have been used previously for ALA studies in oral, bladder, and head and neck tissues[31,41,48] to account for the contribution of endogenous fluorescence. Fluorometric ratios of red fluorescence to green or blue fluorescence were able to detect malignancies in these various organ sites.[31,41,48] However, implementing these methods to account for endogenous fluorescence in the present study did not produce statistically significant differences in the breast cancer cell lines compared to the normal mammary epithelial lines. The probable reason for the lack of significant differences in this study was that the high endogenous fluorescence in the green or blue wavelength range overwhelms the red PpIX contribution. Instead of calculating the ratio in the blue or green, decoupling PpIX fluorescence from the overall remitted fluorescence to compute fractional PpIX fluorescence contribution was required for discrimination of normal mammary epithelium from all breast cancer cell lines and could be completed with a single post-treatment spectroscopic measurement.

Spectroscopic approaches similar to that presented here for separating PpIX fluorescence from endogenous tissue fluorescence has been previously reported by Klinteberg et al.,[21] who used a similar technique for separation of PpIX fluorescence from tissue autofluorescence in photodynamic therapy of basal cell carcinoma. The endogenous fluorescence was removed by exponentially fitting the FAD fluorescence and then subtracting the FAD signal out to determine the photoproducts after photodynamic therapy. Also, spectroscopic deconvolution of the endogenous signal from PpIX spectra has been previously shown by Gibbs-Strauss et al.[49] Comparison of the detected signals to a liquid tissue phantom containing PpIX allowed for delineation of the PpIX signal from nonspecific fluorescence transmitted through normal and cancerous tissue in a mouse brain.[49] The results from the study by Gibbs-Strauss et al.[49] provided evidence of high endogenous fluorescence background when measuring PpIX fluorescence from ALA-treated cancer.

The breast cancer cell lines in this study exhibited a significant increase in fluorescence intensity compared to normal mammary epithelial cells after administration of ALA, as seen previously *in vitro*.[16,23,29] Only one other *in vitro* study has compared PpIX production in a breast cancer and corresponding normal cell line. Specifically, Rodriguez et al.[29] showed that HB4-A R-ras breast cancer cell lines had higher PpIX fluorescence compared to immortalized cells not transfected with the Ras oncogene.

The cellular origin of the MDA-MB-435 cell line has recently been questioned. It has previously been shown that the MDA-MB-435 has a gene-expression profile consistent with M14 melanoma cells.[50] However, more recently it has been argued that the MDA-MB-435 cell line is indeed of breast cancer origin.[51] The MDA-MB-435 originated from a female, and the original M14 melanoma line was reported to be derived from a male patient.[51] The current M14 melanoma line stock does not contain a Y chromosome, which indicates that the M14 was most likely compromised.[51] In spite of the controversy surrounding the origin of the MDA-MB-435 cell line, the results from this study demonstrate concordance between MDA-MB-435 and the other breast cancer cell lines studied in terms of its uptake of ALA.

This paper presents an examination of the diagnostic potential of PpIX with a panel of normal mammary epithelial and breast cancer cell lines. It was found that the relative change in PpIX fluorescence intensity could discriminate breast cancer from normal mammary epithelial cell lines and was not affected by varying ER expression in cell lines. The ability to discriminate cells post-ALA treatment shows the potential for the use of spectroscopic methods in margin assessment of breast cancer with PpIX fluorescence, regardless of ER status. The MDA-MB-361 cell line tested here also expressed the HER2+/NEU phenotype model, but did not have a significantly different PpIX fluorescence intensity as compared to all other cancer cells tested. Therefore, HER2+/NEU cell lines were not further explored by our group, and we believe PpIX would have similar results in other phenotypes, as shown by the lack of difference in the HER2+/NEU phenotype MDA-MB-361 cells.

This study is an important initial step in characterizing PpIX fluorescence expression within different biological subtypes of breast cancer cell lines and comparing them to nor-

mal mammary epithelial cell lines. Because of the limitations of an *in vitro* study, it was not possible to evaluate the possible effects of vascular transport of ALA to the target tissues and the corresponding effect on uptake of ALA and conversion to PpIX. Thus, further work is required to address this issue, and the work presented here is a first step toward realizing the utility of ALA for breast cancer delineation. In future studies, ALA-induced PpIX fluorescence will be examined in xenograft breast cancer models, including ER and HER2+/NEU phenotypes.

Acknowledgments

The authors acknowledge the support of the NIH Imaging Training Grant and DOD Grant No. W81XWH-05-1-0363. The authors also acknowledge the intellectual input and financial support of GE Global Research Center and state that no conflict of interest exists.

References

1. N. Cabioglu, K. Hunt, A. Sahin, and H. Kuerer, "Role for intraoperative margin assessment in patients undergoing breast-conserving surgery," *Ann. Surg. Oncol.* **14**, 1458–1471 (2007).
2. M. R. Bani, M. P. Lux, K. Heusinger, E. Wenkel, A. Magener, R. Schulz-Wendtland, M. W. Beckmann, and P. A. Fasching, "Factors correlating with reexcision after breast-conserving therapy," *Eur. J. Surg. Oncol.* **35**(1), 32–37 (2009).
3. M. F. Dillon, E. W. Mc Dermott, A. O'Doherty, C. M. Quinn, A. D. Hill, and N. O'Higgins, "Factors affecting successful breast conservation for ductal carcinoma *in situ*," *Ann. Surg. Oncol.* **14**(5), 1618–28 (2007).
4. B. D. Florentine, N. K. Kaushal, M. R. Puig, N. Sarda, G. Senofsky, B. T. Cooper, A. Black, R. Zimmerman, and J. Barstis, "Breast-conservation treatment outcomes: a community hospital's experience," *Breast J.* **15**(1), 76–84 (2009).
5. T. L. Huston, R. Pigalarga, M. P. Osborne, and E. Tousimis, "The influence of additional surgical margins on the total specimen volume excised and the reoperative rate after breast-conserving surgery," *Am. J. Surg.* **192**(4), 509–512 (2006).
6. E. D. Kurniawan, M. H. Wong, I. Windle, A. Rose, A. Mou, M. Buchanan, J. P. Collins, J. A. Miller, R. L. Gruen, and G. B. Mann, "Predictors of surgical margin status in breast-conserving surgery within a breast screening program," *Ann. Surg. Oncol.* **15**(9), 2542–2549 (2008).
7. S. A. McLaughlin, L. M. Ochoa-Frongia, S. M. Patil, H. S. Cody, 3rd, and L. M. Sclafani, "Influence of frozen-section analysis of sentinel lymph node and lumpectomy margin status on reoperation rates in patients undergoing breast-conservation therapy," *J. Am. Coll. Surg.* **206**(1), 76–82 (2008).
8. J. E. Mendez, W. W. Lamorte, A. de Las Morenas, S. Cerda, R. Pistey, T. King, M. Kavanah, E. Hirsch, and M. D. Stone, "Influence of breast cancer margin assessment method on the rates of positive margins and residual carcinoma," *Am. J. Surg.* **192**(4), 538–540 (2006).
9. T. S. Menes, P. I. Tartter, I. Bleiweiss, J. H. Godbold, A. Estabrook, and S. R. Smith, "The consequence of multiple re-excisions to obtain clear lumpectomy margins in breast cancer patients," *Ann. Surg. Oncol.* **12**(11), 881–885 (2005).
10. J. F. Waljee, E. S. Hu, L. A. Newman, and A. K. Alderman, "Predictors of re-excision among women undergoing breast-conserving surgery for cancer," *Ann. Surg. Oncol.* **15**(5), 1297–1303 (2008).
11. A. W. Lin, N. A. Lewinski, J. L. West, N. J. Halas, and R. A. Drezek, "Optically tunable nanoparticle contrast agents for early cancer detection: model-based analysis of gold nanoshells," *J. Biomed. Opt.* **10**(6), 064035 (2005).
12. K. Sokolov, D. Nida, M. Descour, A. Lacy, M. Levy, B. Hall, S. Dharmawardhane, A. Ellington, B. Korgel, and R. Richards-Kortum, "Molecular optical imaging of therapeutic targets of cancer," *Adv. Cancer Res.* **96**, 299–344 (2007).
13. M. Veiseh, P. Gabikian, S. B. Bahrami, O. Veiseh, M. Zhang, R. C. Hackman, A. C. Ravanpay, M. R. Stroud, Y. Kusuma, S. J. Hansen, D. Kwok, N. M. Munoz, R. W. Sze, W. M. Grady, N. M. Greenberg, R. G. Ellenbogen, and J. M. Olson, "Tumor paint: a chlorotoxin:Cy5.5 bioconjugate for intraoperative visualization of cancer foci," *Cancer Res.* **67**(14), 6882–6888 (2007).
14. E. Uzgiris, A. Sood, K. Bove, B. Grimmond, D. Lee, and S. Lomnes, "A multimodal contrast agent for preoperative MR imaging and intraoperative tumor margin delineation," *Technol. Cancer Res. Treat.* **5**(4), 301–309 (2006).
15. K. A. Frei, H. M. Bonel, H. Frick, H. Walt, and R. A. Steiner, "Photodynamic detection of diseased axillary sentinel lymph node after oral application of aminolevulinic acid in patients with breast cancer," *Br. J. Cancer* **90**(4), 805–809 (2004).
16. E. R. Gallegos, I. DeLeon Rodriguez, L. A. Martinez Guzman, and A. J. Perez Zapata, "*In vitro* study of biosynthesis of protoporphyrin IX induced by delta-aminolevulinic acid in normal and cancerous cells of the human cervix," *Arch. Med. Res.* **30**(3), 163–170 (1999).
17. F. Gamarra, S. Wagner, S. Al-Batran, I. Maier, M. Castro, H. Hautmann, A. Bergner, R. Baumgartner, and R. M. Huber, "Kinetics of 5-aminolevulinic acid-induced fluorescence in organ cultures of bronchial epithelium and tumor," *Respiration* **69**(5), 445–450 (2002).
18. S. L. Gibbs, B. Chen, J. A. O'Hara, P. J. Hoopes, T. Hasan, and B. W. Pogue, "Protoporphyrin IX level correlates with number of mitochondria, but increase in production correlates with tumor cell size," *Photochem. Photobiol.* **82**(5), 1334–1341 (2006).
19. H. Hirschberg, D. Sorensen, E. Angell-Petersen, Q. Peng, B. Tromberg, C. Sun, S. Spetalen, and M. S, "Repetitive photodynamic therapy of malignant brain tumors," *J. Environ. Pathol. Toxicol. Oncol.* **25**(1–2), 261–279. (2006).
20. Z. Ji, G. Yang, V. Vasovic, B. Cunderlikova, Z. Suo, J. M. Nesland, and Q. Peng, "Subcellular localization pattern of protoporphyrin IX is an important determinant for its photodynamic efficiency of human carcinoma and normal cell lines," *J. Photochem. Photobiol., B* **84**(3), 213–220 (2006).
21. C. Klinteberg, A. Enejder, I. Wang, S. Andersson-Engels, S. Svanberg, and K. Svanberg, "Kinetic fluorescence studies of 5-aminolaevulinic acid-induced protoporphyrin IX accumulation in basal cell carcinomas," *J. Photochem. Photobiol. B: Biol.* **49**, 120–128 (1999).
22. B. Krammer and K. Plaetzer, "ALA and its clinical impact from benchside to bedside," *Photochem. Photobiol. Sci.* **7**(3), 283–289 (2008).
23. R. C. Krieg, H. Messmann, J. Rauch, S. Seeger, and R. Knuechel, "Metabolic characterization of tumor cell-specific protoporphyrin IX accumulation after exposure to 5-aminolevulinic acid in human colonic cells," *Photochem. Photobiol.* **76**(5), 518–525 (2002).
24. D. P. Ladner, R. A. Steiner, J. Allemann, U. Haller, and H. Walt, "Photodynamic diagnosis of breast tumours after oral application of aminolevulinic acid," *Br. J. Cancer* **84**(1), 33–37 (2001).
25. A. Leunig, K. Rick, H. Stepp, R. Gutmann, G. Alwin, R. Baumgartner, and J. Feyh, "Fluorescence imaging and spectroscopy of 5-aminolevulinic acid induced protoporphyrin IX for the detection of neoplastic lesions in the oral cavity," *Am. J. Surg.* **172**(6), 674–677 (1996).
26. H. Messmann, R. Knuchel, W. Baumier, A. Holstege, and J. Scholmerich, "Endoscopic fluorescence detection of dysplasia in patients with Barrett's esophagus, ulcerative colitis, or adenomatous polyps after 5-aminolevulinic acid-induced protoporphyrin IX sensitization," *Gastrointest. Endosc.* **49**(1), 1–5 (1999).
27. R. Na, I. Stender, and H. Wulf, "Can autofluorescence demarcate basal cell carcinoma from normal skin? A comparison with protoporphyrin IX fluorescence," *Acta Derm Venereol* **81**, 246–249 (2001).
28. N. Navone, C. Polo, A. Frisardi, N. Andrade, and A. Battle, "Heme biosynthesis in human breast cancer—mimetic *in vitro* studies and some heme enzymic activity levels," *Int. J. Biochem.* **22**(12), 1407–1411 (1990).
29. L. Rodriguez, G. Divenosa, A. Batlle, A. Macrobert, and A. Casas, "Response to ALA-based PDT in an immortalised normal breast cell line and its counterpart transformed with the Ras oncogene," *Photochem. Photobiol. Sci.* **6**(12), 1306–1310 (2007).
30. R. Sailer, W. S. Strauss, M. Wagner, H. Emmert, and H. Schneckenburger, "Relation between intracellular location and photodynamic efficacy of 5-aminolevulinic acid-induced protoporphyrin IX *in vitro*. Comparison between human glioblastoma cells and other cancer cell lines," *Photochem. Photobiol. Sci.* **6**(2), 145–151 (2007).
31. A. Sharwani, W. Jerjes, V. Salih, A. J. MacRobert, M. El-Maaytah, H.

S. Khalil, and C. Hopper, "Fluorescence spectroscopy combined with 5-aminolevulinic acid-induced protoporphyrin IX fluorescence in detecting oral premalignancy," *J. Photochem. Photobiol., B* **83**(1), 27–33 (2006).
32. K. T. Moesta, B. Ebert, T. Handke, D. Nolte, C. Nowak, W. E. Haensch, R. K. Pandey, T. J. Dougherty, H. Rinneberg, and P. M. Schlag, "Protoporphyrin IX occurs naturally in colorectal cancers and their metastases," *Cancer Res.* **61**(3), 991–999 (2001).
33. S. Andersson-Engels, G. Canti, R. Cubeddu, C. Eker, C. Klinteberg, A. Pifferi, K. Svanberg, S. Svanberg, P. Taroni, G. Valentini, and I. Wang, "Preliminary evaluation of two fluorescence imaging methods for the detection and the delineation of basal cell carcinomas of the skin," *Lasers Surg. Med.* **26**(1), 76–82 (2000).
34. C. S. Betz, H. Stepp, P. Janda, S. Arbogast, G. Grevers, R. Baumgartner, and A. Leunig, "A comparative study of normal inspection, autofluorescence and 5-ALA-induced PPIX fluorescence for oral cancer diagnosis," *Int. J. Cancer* **97**(2), 245–252 (2002).
35. J. Y. Chen, N. Q. Mak, N. H. Cheung, R. N. Leung, and Q. Peng, "Endogenous production of protoporphyrin IX induced by 5-aminolevulinic acid in leukemia cells," *Acta Pharmacol. Sin.* **22**(2), 163–168 (2001).
36. A. M. Dorward, K. S. Fancher, T. M. Duffy, W. G. Beamer, and H. Walt, "Early neoplastic and metastatic mammary tumours of transgenic mice detected by 5-aminolevulinic acid-stimulated protoporphyrin IX accumulation," *Br. J. Cancer* **93**(10), 1137–1143 (2005).
37. N. Fotinos, M. A. Campo, F. Popowycz, R. Gurny, and N. Lange, "5-Aminolevulinic acid derivatives in photomedicine: Characteristics, application and perspectives," *Photochem. Photobiol.* **82**(4), 994–1015 (2006).
38. Y. Berger, C. Chapuis Bernasconi, F. Schmitt, R. Neier, and L. Juillerat-Jeanneret, "Determination of intracellular prolyl/glycyl proteases in intact living human cells and protoporphyrin IX production as a reporter system," *Chem. Biol.* **12**(8), 867–872 (2005).
39. M. G. Alvarez, M. S. Lacelli, V. Rivarola, A. Batlle, and H. Fukuda, "5-aminolevulinic acid-mediated photodynamic therapy on Hep-2 and MCF-7c3 cells," *J. Environ. Pathol. Toxicol. Oncol.* **26**(2), 75–82 (2007).
40. S. Wu, Q. Ren, M. Zhou, Y. Wei, and J. Chen, "Photodynamic effects of 5-aminolevulinic acid and its hexylester on several cell lines," *Sheng Wu Hua Xue Yu Shen Wu Wu Li Xue Bao* **35**(7), 655–660 (2003).
41. D. Zaak, D. Frimberger, H. Stepp, S. Wagner, R. Baumgartner, P. Schneede, M. Siebels, R. Knuchel, M. Kriegmair, and A. Hofstetter, "Quantification of 5-aminolevulinic acid induced fluorescenc improves the specificity of bladder cancer detection," *J. Urol. (Baltimore)* **166**(5), 1665–1668 (2001).
42. European Public Assessment Report: Gliolan Available from ⟨http://www.emea.europa.eu/humandocs/PDFs/EPAR/gliolan/H-744-en1.pdf⟩ (2007).
43. T. Tsai, H. T. Ji, P. C. Chiang, R. H. Chou, W. S. Chang, and C. T. Chen, "ALA-PDT results in phenotypic changes and decreased cellular invasion in surviving cancer cells," *Lasers Surg. Med.* **41**(4), 305–315 (2009).
44. S. Anandappa, R. Sibson, A. Platt-Higgins, J. Winstanley, P. Rudland, and R. Barraclough, "Variant estrogen receptor alpha mRNAs in human breast cancer specimens," *Int. J. Cancer* **88**, 209–216 (2000).
45. ⟨www.protocol-online.org/biology-forums/posts/5763.htm⟩ (2008).
46. R. S. DaCosta, H. Andersson, and B. C. Wilson, "Molecular fluorescence excitation-emission matrices relevant to tissue spectroscopy," *Photochem. Photobiol.* **78**(4), 384–392 (2003).
47. E. C. Dietze, M. M. Troch, G. R. Bean, J. B. Heffner, M. L. Bowie, P. Rosenberg, B. Ratliff, and V. L. Seewaldt, "Tamoxifen and tamoxifen ethyl bromide induce apoptosis in acutely damaged mammary epithelial cells through modulation of AKT activity," *Oncogene* **23**(21), 3851–3862 (2004).
48. I. Wang, L. Clemente, R. Pratas, E. Cardoso, M. Clemente, S. Montan, S. Svanberg, and K. Svanberg, "Fluorescence diagnostics and kinetics studies in the head and neck region utilizing low-dose d-aminolevulinic acid sensitization," *Cancer Lett.* **135**(11–9), 1–8 (1999).
49. S. L. Gibbs-Strauss, J. A. O'Hara, P. J. Hoopes, T. Hasan, and B. W. Pogue, "Noninvasive measurement of aminolevulinic acid-induced protoporphyrin IX fluorescence allowing detection of murine glioma *in vivo*," *J. Biomed. Opt.* **14**(1), 014007 (2009).
50. J. M. Rae, C. J. Creighton, J. M. Meck, B. R. Haddad, and M. D. Johnson, "MDA-MB-435 are derived from M-14 melanoma cells-a loss for breast cancer, but a boon for melanoma research," *Breast Cancer Res. Treat.* **104**(1), 13–19 (2007).
51. A. F. Chambers, "MDA-MB-435 and M14 cell lines: Identical but not M14 melanoma?" *Cancer Res.* **69**(13), 5292–5293 (2009).

Breast Cancer Res Treat (2011) 126:55–62
DOI 10.1007/s10549-010-0884-1

PRECLINICAL STUDY

Uptake of 2-NBDG as a method to monitor therapy response in breast cancer cell lines

Stacy R. Millon · Julie H. Ostrander · J. Quincy Brown · Anita Raheja · Victoria L. Seewaldt · Nirmala Ramanujam

Received: 25 January 2010 / Accepted: 1 April 2010 / Published online: 14 April 2010

Abstract This study quantifies uptake of a fluorescent glucose analog, (2-(*N*-(7-nitrobenz-2-oxa-1,3-diazol-4-yl)amino)-2-deoxyglucose) (2-NBDG), in a large panel of breast cancer cells and demonstrates potential to monitor changes in glycolysis caused by anticancer and endocrine therapies. Expressions of glucose transporter (GLUT 1) and hexokinase (HK I), which phosphorylates 2-NBDG, were measured via western blot in two normal mammary epithelial and eight breast cancer cell lines of varying biological subtype. Fluorescence intensity of each cell line labeled with 100 μM 2-NBDG for 20 min or unlabeled control was quantified. A subset of cancer cells was treated with anticancer and endocrine therapies, and 2-NBDG fluorescence changes were measured. Expression of GLUT 1 was necessary for uptake of 2-NBDG, as demonstrated by lack of 2-NBDG uptake in normal human mammary epithelial cells (HMECs). GLUT 1 expression and 2-NBDG uptake was ubiquitous among all breast cancer lines. Reduction and stimulation of 2-NBDG uptake was demonstrated by perturbation with anticancer agents, lonidamine (LND), and α-cyano-hydroxycinnamate (α-Cinn), respectively. LND directly inhibits HK and significantly reduced 2-NBDG fluorescence in a subset of two breast cancer cell lines. Conversely, when cells were treated with α-Cinn, a drug used to increase glycolysis, 2-NBDG uptake was increased. Furthermore, tamoxifen (tam), a common endocrine therapy, was administered to estrogen receptor positive and negative (ER+/−) breast cells and demonstrated a decreased 2-NBDG uptake in ER+ cells, reflecting a decrease in glycolysis. Results indicate that 2-NBDG uptake can be used to measure changes in glycolysis and has potential for use in early drug development.

Keywords 2-NBDG · Breast cancer cell lines · Confocal microscopy · GLUT 1 · Tamoxifen

S. R. Millon (✉) · J. Q. Brown · A. Raheja · N. Ramanujam
Department of Biomedical Engineering, Duke University, 136 Hudson Hall, Campus, Box 90281, Durham, NC 27708-0281, USA
e-mail: stacy.millon@duke.edu

J. H. Ostrander · V. L. Seewaldt
Department of Medicine, Duke University, Durham, NC, USA

Introduction

Functional imaging of glucose uptake has been shown to be invaluable in breast cancer diagnosis, prognosis, and therapy monitoring [1]. Many cancers demonstrate aerobic glycolysis, glucose metabolism in the presence of oxygen [1–3]. Current methods to measure glycolysis include measurement of dielectric response [4], protein quantification [5], nuclear resonance and imaging [1, 6, 7], microarray quantification [8], and pH responsive dyes [9]. Monitoring glycolysis is most commonly measured with fluoro-deoxyglucose (FDG), a radioactive glucose analog, and is detected with Positron Emission Tomography (PET) [1]. All of these techniques, however, can be prohibitively expensive, manually intensive, and/or technologically complex rendering them impractical for high-throughput drug development even with demonstration of clinical success [1].

2-(*N*-(7-nitrobenz-2-oxa-1,3-diazol-4-yl)amino)-2-deoxyglucose (2-NBDG) is an optical contrast agent that follows a similar metabolic pathway to D-glucose [3]. 2-NBDG enters the cell via glucose transporters (GLUT), and is

phosphorylated at the C-6 position by hexokinases I–II (HK) [3]. The phosphorylated fluorescent metabolite 2-NBDG-6-phosphate remains in the cell until further decomposition occurs into a non-fluorescent form [10]. 2-NBDG can be maximally excited at 488 nm and emits at 540 nm. Cellular glycolysis and the proteins GLUT 1 and HK I have all previously been shown to be up regulated in breast cancer [11] and thus, it would be expected that increased glycolysis would lead to increased accumulation of 2-NBDG in malignant relative to benign tissues [2, 3].

Previous studies to examine applications of 2-NBDG have focused on cancer detection in vivo [12], on ex vivo tissue [2], or in vitro [3, 13]. Preferential accumulation of 2-NBDG in cancer tissue over surrounding normal tissue was demonstrated to be 3.7× higher in 20 neoplastic ex vivo oral biopsy specimens compared to matched normal tissue biopsies [2]. Sheth et al. demonstrated the pre-clinical utility of 2-NBDG in several in vivo mouse models, demonstrating 2-NBDG uptake was greater in a fasting (glucose deprived) animal compared to a non-fasting animal, was co-localized with RFP in a gliosarcoma tumor within a period of 60 min (Warburg Effect) and demonstrated preferential uptake in a stimulated seizure model of the brain as compared to one that was free of seizures [12].

Preferential uptake of 2-NBDG in breast cancer has been carried out previously on in vitro cell studies, but not in pre-clinical models of breast cancers or human breast cancers. O'Neil et al. demonstrated a 3.5× greater uptake of 2-NBDG in MCF7 cells as compared to non-malignant M-1 epithelial cells following 10 min of incubation in 0.3 mM concentration of the contrast agent [3]. Levi et al. used MCF7, MDA-MB-435, and MDA-MB-231 cell lines to compare 2-NBDG uptake at 10 μM to 10 μM of NIR-fructose uptake after 15 min of incubation and found them to be equivalent [13].

(2-(*N*-(7-nitrobenz-2-oxa-1,3-diazol-4-yl)amino)-2-deoxyglucose) could play an important role in in vitro cell line studies. 2-NBDG allows for the evaluation of the efficacy of drugs on a large number of different cell lines, which is particularly important given the heterogeneity of breast disease. The objective of the study reported here was to demonstrate the utility of 2-NBDG as a molecular contrast agent to quantitatively measure changes in glycolysis and to demonstrate a method to measure the response of breast cancer cell lines to therapy. Confocal microscopy was used to image the fluorescence signal from 2-NBDG in a panel of 10 different breast cell lines—two normal mammary epithelial and eight cancer that included estrogen receptor positive (ER+) and negative (ER−) cell lines. The expression of GLUT 1 and HK I proteins were quantified following western blot analysis and compared to fluorescence results obtained from these cells. A subset of two breast cancer cell lines was then treated with anticancer therapies that directly affect glycolysis: lonidamine (LND), a HK inhibitor, and α-cyano-hydroxycinnamate (α-Cinn), a glycolytic stimulator, to demonstrate the ability to measure opposing perturbations on 2-NBDG uptake. Finally, a subset of 1 ER+ and 1 ER− breast cancer cell lines was treated with a therapeutic dose of tamoxifen (tam), a widely used endocrine therapy for treatment of patients with ER+ breast cancer, to determine if the changes in 2-NBDG uptake are consistent with the expected effects of tam, a reduction in glycolysis.

Methods and materials

Cell culture

Two cell lines were derived from the normal mammary epithelium (MCF12 and human mammary epithelial cells (HMEC)), and eight were derived from patients with breast cancer (BT-20, BT-474, MDA-MB-231, MDA-MB-361, MDA-MB-435, MDA-MB-468, MCF7, and T47D). Breast cancer cell lines and the MCF12 cell line were obtained from the American Type Culture collection, ATCC (Manassas, VA, USA). Primary HMECs were obtained from Lonza (Basel, Switzerland) and infected with a retrovirus encoding human telomerase reverse transcriptase (hTERT) for immortalization. All cells remained free of contaminants and were propagated by adherent culture, trypsinized, and plated according to established protocols [14, 15]. Cells were plated at 100,000 cells/ml in 10 ml for western blot analysis and 2 ml for all confocal imaging studies.

Confocal microscopy parameters

All confocal images were collected on a Leica SP5 laser scanning confocal microscope (Wetzlar, Germany) using a previously published protocol [15]. Briefly, a 488-nm argon laser source (power at sample was 3.5 mW) was coupled to an inverted Leica DM16000CS microscope with a 40× oil-immersion objective (Leica Plan NeoFluor, NA = 1.25). Emission was collected at 515–585 nm, chosen from preliminary spectroscopy data on MCF7 cells to incorporate the full-width half-maximum of 2-NBDG. Images were acquired with a PMT gain of 950 V, offset 0.7%, and zoom of 1.6 to measure the unlabeled and labeled 2-NBDG cells. This gain was chosen for quantification of weakly fluorescent unlabeled cells to allow comparison to 2-NBDG-labeled cells. Images of anticancer and endocrine therapy treated and vehicle control cells (all 2-NBDG labeled) were acquired with a gain of 750 V, offset 0.7%, and zoom of 1.6. The gain was lowered since some 2-NBDG labeled cell lines had saturated pixels in the first set of experiments, specifically MDA-MB-435.

Cell imaging studies

Overall uptake of 2-NBDG (2-NBDG labeled versus unlabeled) was quantified for all 10 breast cell lines and then a new set of experiments was conducted for each anticancer or endocrine treatment (treated versus vehicle control). Each sample was defined as the average intensity of all cells within a single confocal image. The imaging field of view was 242 μm × 242 μm with 512 × 512 pixels per image. Two samples were acquired per plate. Sample sizes for each cell line included four, 2-NBDG labeled and four unlabeled plates. All 10 cell lines were tested in the unlabeled versus labeled experiments, and MDA-MB-435 and MDA-MB-468 cells were tested with anticancer agents (LND and α-Cinn) and MCF7 (ER+) and MDA-MB-435 (ER−) with endocrine therapy (tamoxifen).

2-NBDG uptake

Confocal microscopy imaging sessions were carried out 24 h after plating in the first experimental set that tested 2-NBDG uptake in all breast cell lines or after the treatment periods of 48 or 72 h, for the anticancer and endocrine therapies, respectively. The original cell media was removed from each dish, and cells were washed twice with PBS. Cells were labeled with either 100 μM 2-NBDG dissolved in glucose-free cell media, or glucose-free media alone for unlabeled cells, and incubated for 20 min. The media was then removed and the cells were washed 3 times with PBS and imaged. The concentration of 2-NBDG used was based on initial studies on two plates each of HMEC and MCF7 cell lines (data not shown). Cells, at 2-NBDG concentrations of 25, 50, 100, and 200 μM, were incubated with 2-NBDG for 20 min and were compared to equivalent unlabeled cells. Intracellular 2-NBDG fluorescence increased approximately linearly with concentration. However, at a concentration of 200 μM the fluorescence of most cells saturated the microscope detector. Therefore, a concentration in the middle of the tested range and equivalent to that used in previous cell studies [3], 100 μM, was chosen for subsequent studies. To determine the optimal time to measure 2-NBDG fluorescence (data not shown), two plates each of MCF7 and HMEC cells were tested at 10, 20 and 45 min. Fluorescence intensity was found to be significantly different after 20 min ($P < 0.05$) between 2-NBDG labeled and unlabeled cells and results matched previous studies at this time point [3].

Anticancer and endocrine treatments

A subset of cells (MDA-MB-435 and MDA-MB-468) was treated with the anticancer agents, LND, and α-cyano-hydroxycinnamate (α-Cinn). These cell lines were chosen since they both expressed HK I protein on a western blot ("Results"), and each cell line possesses unmethylated monocarboxylate transporter 1 (MCT1), which is the transporter that is blocked by α-Cinn [16]. Twenty-four hours after plating, cells were treated with 600 μM LND or 840 μM α-Cinn dissolved in dimethyl sulfoxide (DMSO) for 48 h [17]. The corresponding vehicle control was treated with DMSO only. Tam treatment was carried out at a concentration of 2 μM for 72 h, and the corresponding vehicle control was ethanol. G1 cell cycle arrest was determined via cell cycle analysis to occur in MCF7 cells after treatment with tam. After treatment, the cells were then labeled with 2-NBDG according to the protocol discussed and imaged at the settings described.

Data processing

Fluorescence intensity images were analyzed using NIH ImageJ software and analyzed with methods published previously [15]. Briefly, fluorescence intensity for each breast cell line was determined by manually segmenting each cell in the image and then computing the average fluorescence intensity for all cells in the image. Background intensity was subtracted and the resulting data normalized by a fluorescence calibration standard, which consisted of a fluorescent bead (FocalCheck Fluorescence Microscope Test Slide #2, Invitrogen, Carlsbad, CA, USA), measured daily to account for small changes in laser power. A total of $n = 8$ fields of view per cell line (two per sample per experimental arm) were imaged from which the average integrated fluorescence intensity per cell line was derived.

Western blots

Western blots were carried out according to standard procedures [18]. Briefly, after lysing the cells, resultant protein samples were heated to 95°C for 5 min and subjected to sodium dodecyl sulfate–polyacrylamide gel electrophoresis on 4–12% gradient 1-mm acrylamide gels, followed by transfer to polyvinylidene difluoride membranes for 1.5 h at 150 V with a NOVEX semi-transfer unit. Membranes were blocked for 1.5 h in Tris-buffered saline with 0.01% Tween 20, and incubated overnight with primary antibody: rabbit polyclonal GLUT 1 antibody or mouse monoclonal HK I antibody (Santa Barbara Biotech, California) in Tris-buffered saline with 0.01% Tween 20 with 10% bovine serum albumin. One hour incubation with horseradish peroxidase-conjugated anti-rabbit or mouse antibody, respectively, (Santa Barbara Biotech, California) followed. Blots were developed with an enhanced chemiluminescence kit (Amersham Pharmacia Biotech, Piscataway, NJ), and band intensity was quantified on the image by

manually circling signal area from blot background (Eastman Kodak Co., Rochester, NY). Signal was discriminated with a threshold determined from an 8-color rainbow look up table (signal was determined to be within the green–red coloration).

Statistics

All statistics were computed with JMP (SAS, Cary, NC, USA) software. ANOVAs and *t*-tests were completed with a Tukey–Kramer correction for multiple comparisons to determine statistical significance. Exact two-sided *P*-values were computed, and all $P < 0.05$ were considered significant. All correlations were calculated with a Pearson coefficient.

Results

A variety of breast cancer cells were tested in order to ensure that varying molecular phenotypes did not influence uptake of 2-NBDG. Estrogen receptor (ER), human growth receptor 2 (HER2), and progesterone receptor (PR) status are given for each cell line as reported by ATCC in Table 1.

Western blot results

Expression of GLUT 1 and HK I proteins was determined for all 10 cell lines with actin serving as an internal reference (Fig. 1). It is evident from the results that all malignant cell lines express measurable, but variable, GLUT 1 protein levels while the HMEC strain exhibits a negligible amount of GLUT 1 compared to its malignant counterparts. Interestingly, the other non-malignant epithelial line (MCF12) exhibited measurable levels of GLUT 1. HK I levels are widely variable across malignant cell lines. HMEC cells exhibit nominal levels of HK I when compared to malignant lines. The MCF12 line exhibited fairly high levels of HK I expression when compared to malignant cell lines. Furthermore, high GLUT 1 expression did not necessarily correspond to high HK I expression, as seen in the T47D cell line.

Table 1 Summary of cell lines tested and ER, HER2, and PR receptor status

Cell line	Type	ER	HER 2	PR
MCF12	Normal			
HMEC	Normal			
BT-474	Cancer	+	+	+
T47D	Cancer	+	−	+
MCF7	Cancer	+	−	+
MDA-MB-435	Cancer	−	−	−
BT-20	Cancer	−	−	−
MDA-MB-361	Cancer	+	+	−
MDA-MB-231	Cancer	−	−	−
MDA-MB-468	Cancer	−	−	−

2-NBDG uptake in cells

Figure 2 shows representative fluorescence intensity images of 2-NBDG labeled and unlabeled HMEC (normal) and MDA-MB-435 and MDA-MB-468 (cancer) cell lines. The two cancer cell lines shown were subsequently tested with both anticancer agents (LND and α-Cinn). All cell lines show similar diffusely distributed baseline fluorescence in the cytoplasm (as opposed to the nucleus), which is likely due to flavoproteins. HMEC does not show a significant increase in fluorescence after 2-NBDG labeling. Conversely, labeled breast cancer cell lines are significantly more fluorescent than unlabeled.

Figure 3 shows bar graphs of fluorescence intensity after 2-NBDG labeling for the 10 cell lines, grouped as normal mammary epithelial cells and breast cancer cells. Figure 3a shows mean calibrated fluorescence intensity stratified by cell line. Figure 3b shows Δ change in fluorescence intensity defined as: 2-NBDG labeled intensity − unlabeled fluorescence intensity. All cell lines exhibited significantly greater fluorescence intensity following 2-NBDG labeling ($P < 0.05$). As expected, all breast cancer cell lines had a significantly greater uptake of 2-NBDG than HMEC. MCF12 had an approximate 10-fold increase in 2-NBDG fluorescent intensity over the HMECs (Fig. 3a, b). Significant differences were observed between MCF12 and individual breast cancer cell lines (BT-20 and MDA-MB-468, specifically). When comparing the 2-NBDG fluorescence to the relative GLUT 1 and HK I protein expressions

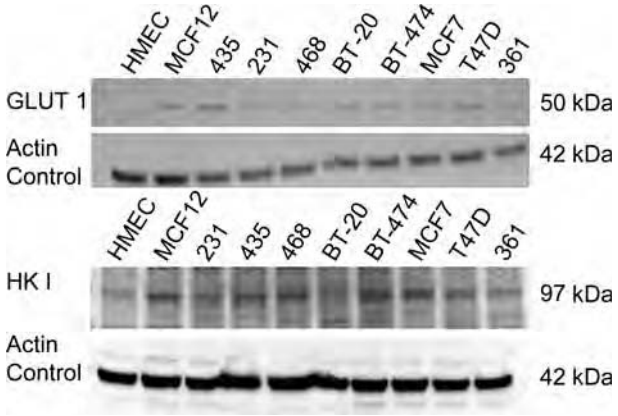

Fig. 1 Western blot analysis of GLUT 1 and HK I levels in 10 breast cancer cells

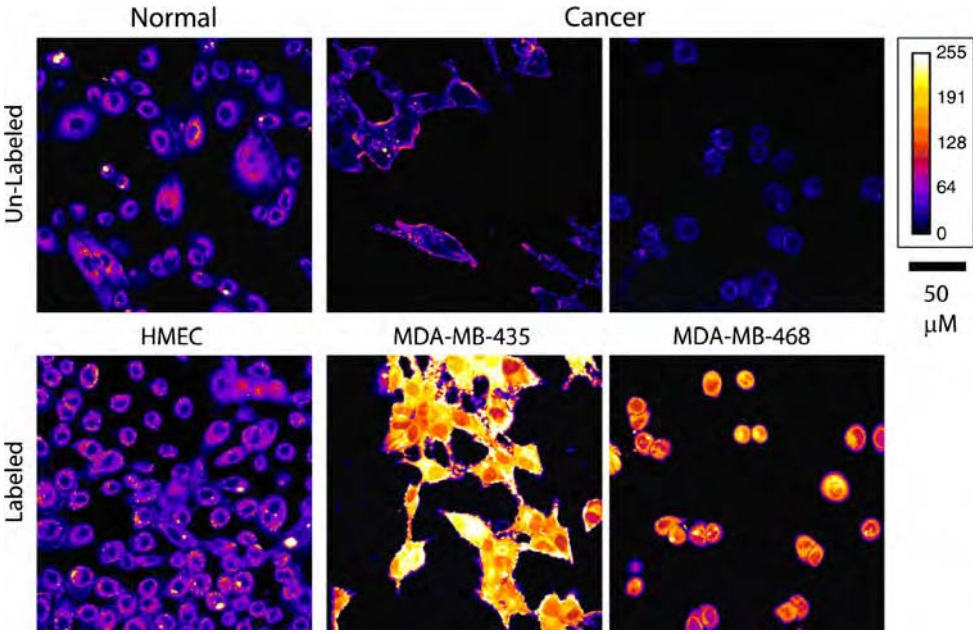

Fig. 2 Representative confocal fluorescence images of normal mammary epithelial and breast cancer cells 2-NBDG labeled and unlabeled. Excitation was at 488 nm, and emission was collected between 515 and 585 nm

shown in the western blot, no linear relationship was observed (Pearson correlation coefficient = 0.44; 0.50, respectively).

2-NBDG uptake after anticancer and endocrine treatments

All breast cancer cell lines demonstrated a significant increase in fluorescence intensity after 2-NBDG labeling. Therefore, a subset of two cell lines (MDA-MB-435 and MDA-MB-468) were treated with LND or α-Cinn to determine if a decrease or increase in glycolysis, respectively, could be measured with 2-NBDG. Figure 4 is a bar graph of the mean calibrated 2-NBDG fluorescence intensity of the two breast cancer cell lines treated with the agents (LND and α-Cinn) and vehicle controls.

Inhibition of HK I by LND demonstrated a significant inhibition of glucose uptake, as indicated by the decreased 2-NBDG fluorescence ($P < 0.05$). MDA-MB-468 demonstrated an approximate 50% decrease in 2-NBDG fluorescence intensity, whereas MDA-MB-435 fluorescence intensity only decreased by 15%. Inhibition of lactate-fueled respiration and subsequent increase in glycolysis via α-Cinn demonstrated the opposite trend. A significant increase in 2-NBDG uptake, as reflected by increased 2-NBDG fluorescence, was observed. MDA-MB-468 demonstrated a greater inhibition of 2-NBDG uptake after LND than MDA-MB-435, but increase in 2-NBDG fluorescence after α-Cinn treatment was similar ($P > 0.05$) between both cell lines. The increase in 2-NBDG fluorescence intensity was 20% and 25% for MDA-MB-468 and MDA-MB-435, respectively. It should be noted that the fluorescence intensity values shown in Fig. 4 cannot be directly compared with the results shown in Fig. 3 since the gain on the microscope was decreased to prevent 2-NBDG-labeled cell intensity from saturating the detector in the case of data collected for Fig. 4.

To ensure that 2-NBDG uptake could be influenced by indirect changes in cellular glycolysis and not only by direct inhibition or stimulation of glycolysis, tam-sensitive (MCF7 which are ER+) and -insensitive cells (MDA-MB-435 which are ER−) were treated with 2 μM tam. Rivenzon-Segal et al. had previously demonstrated GLUT 1 inhibition after 48 and 72 h of 2 μM of tam treatment in vitro [19]. GLUT 1 expression was measured following western blot analysis in tam-treated and vehicle control-treated MCF7 and MDA-MB-435 cell lines (Fig. 5a). Treated MCF7 cells showed a lower GLUT 1 expression as compared to control MCF7 cells, whereas the GLUT 1 expression of MDA-MB-435 cells was unchanged after treatment. The corresponding actin control is shown below GLUT 1. Accordingly, 2-NBDG uptake was significantly decreased in the treated MCF7 (tam-sensitive) cells over control MCF7 cells Fig. 5b. 2-NBDG uptake in MDA-MB-435 (tam-insensitive) cells did not change after treatment in Fig. 5b.

Discussion

This study demonstrates the ability to measure changes in glycolysis with the uptake of 2-NBDG via confocal fluorescence microscopy after anticancer and endocrine therapies. Our results showed that 2-NBDG accumulation in breast cell lines occurs in cells that express GLUT 1 regardless of receptor status. HMEC showed relatively

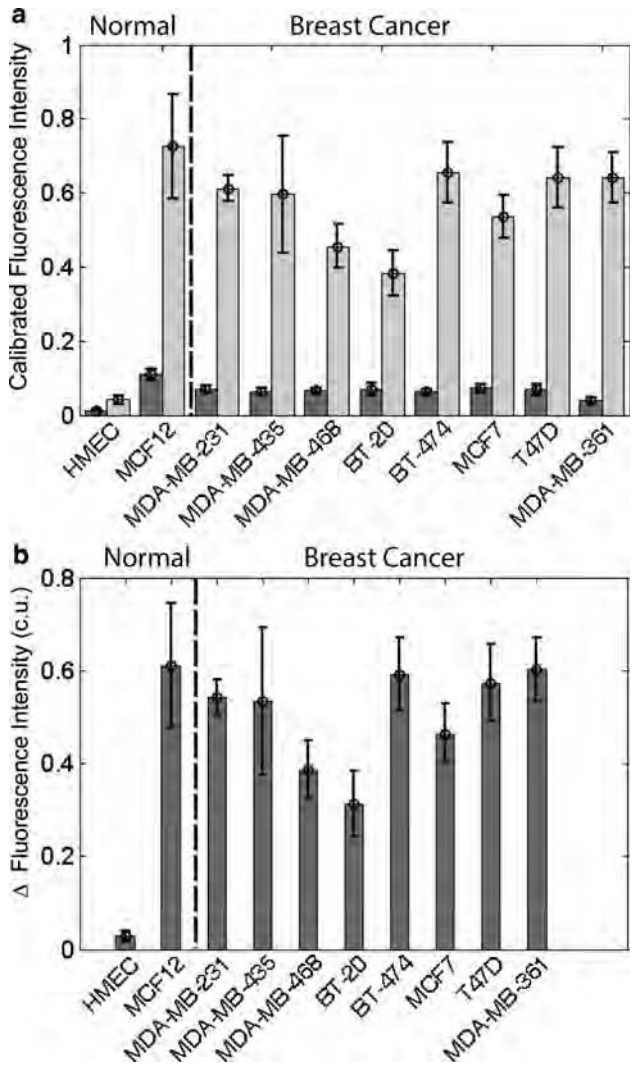

Fig. 3 **a** Mean calibrated fluorescence intensity values and standard deviation of all 10 tested cell lines. **b** Mean Δ change and standard deviation in fluorescence intensity. Note that both cell lines to the left of the *dashed line* in (**a**) and (**b**) are normal mammary epithelial cell lines, and cell lines to the right of the *dashed line* are breast cancer cell lines

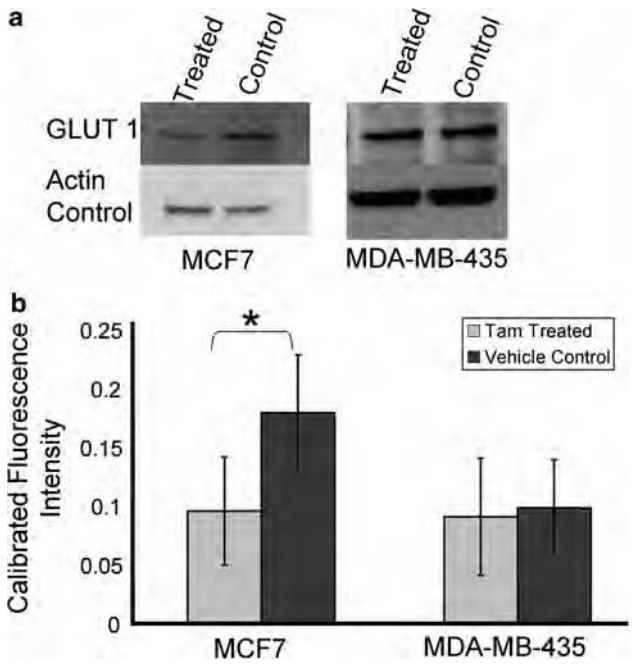

Fig. 5 **a** Western blot of GLUT 1 expression in treated and control MCF7 and MDA-MB-435 cell lines with corresponding actin controls below. **b** Calibrated mean fluorescence intensity values and standard deviation after treatment with tam in MCF7 and MDA-MB-435 cell lines (* denotes $P < 0.05$)

little 2-NBDG uptake, likely due to the very low levels of GLUT 1 expression. Previous in vitro studies carried out with 2-NBDG have shown that GLUT 1 influences competitive uptake using media with D-glucose, a GLUT 1 transporter specific glucose [13]. Our study quantified protein expression of GLUT 1 and HK I and demonstrated that HMEC expressed negligible GLUT 1 and had a significantly lower fluorescence intensity after 2-NBDG labeling. The normal MCF12 cell line, which expressed GLUT 1, took up a significant amount of 2-NBDG, as did all breast cancer cells. GLUT 1 is not typically overexpressed in normal mammary epithelium [11], and we

Fig. 4 **a** Calibrated mean fluorescence intensity values and standard deviation after treatment with LND in MDA-MB-468 and MDA-MB-435 cell lines. **b** Calibrated mean fluorescence intensity values and standard deviation after treatment with α-Cinn in MDA-MB-468 and MDA-MB-435 cell lines (* denotes $P < 0.05$)

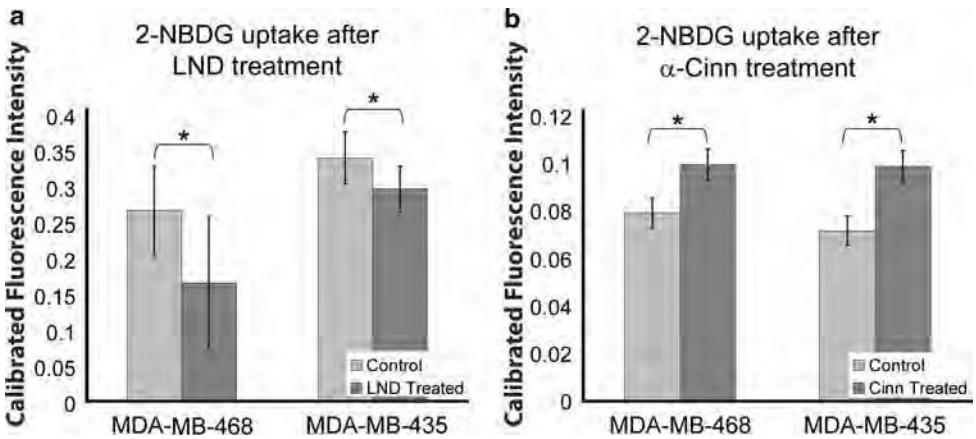

hypothesize GLUT 1 expression likely occurred during immortalization of MCF12.

A large panel of breast cancer cells was investigated to ensure that 2-NBDG could be used ubiquitously; all breast cancer cells demonstrated the ability to uptake 2-NBDG. However, variations in overall uptake could be seen between cell lines. It is believed to be due to differences in GLUT 1 and HK I expression and kinetics of 2-NBDG uptake in each cell line, which was not tested in this study. Only two cell lines were used to determine the optimal time point to examine 2-NBDG uptake. The uptake time of 20 min was chosen in order to be able to image the significant contrast between 2-NBDG labeled and unlabeled cells reasonably immediately.

Increasingly, drugs are being developed to target glycolysis [20]. To demonstrate 2-NBDG applicability to monitor breast cancer response to therapy, agents that directly inhibit and stimulate glycolysis were used on a subset of breast cancer cell lines. HK I protein, which is critical for glucose metabolism, was expressed in all cell lines. HK I has previously been demonstrated to be influential in the uptake of FDG [11]. GLUT 1 was expressed in all cells lines except in the HMECs. GLUT 1 has been previously shown to be over-expressed in breast cancer [21]. GLUT 1 and HK I did not directly correlate with the uptake of 2-NBDG in the breast cancer cell lines tested here. This could potentially be due to the fact that western blots are a measure of protein expression, and not the activity level. Also, several GLUT exist within the cell membranes that transport glucose, such as GLUT 2.

The importance of HK I was demonstrated by directly inhibiting it with the anticancer agent, LND [22]. LND decreased 2-NBDG uptake by inhibiting HK I. The greater inhibition in the uptake of 2-NBDG after LND treatment in MDA-MB-468 is believed to be due to the higher expression of HK I. However, from these studies it is difficult to explain specifically the basis for the differences in 2-NBDG uptake between the two cell lines. Possible sources for these differences could include overall kinetics of the pathways, protein activity within the cells, or dosage. Further experiments are needed to fully elucidate these differences. Nonetheless, a change in 2-NBDG uptake due to inhibition of HK has not been previously demonstrated. To ensure that inhibition of 2-NBDG uptake was not caused by the presence of the LND molecule, α-Cinn was also tested. α-Cinn has been previously shown in 2-NBDG studies to increase 2-NBDG uptake in neurons [16] and increase glucose use in SiHa cells [23], and therefore, α-Cinn should be able to demonstrate the stimulation of 2-NBDG uptake in breast cancer. The opposing trends in 2-NBDG uptake seen with treatment using α-Cinn also confirm that inhibition of LND is not caused by just the presence of the molecule and that 2-NBDG can be used to monitor stimulation or inhibition of glycolysis.

Vehicle controls shown in Fig. 4 have 200 μM DMSO and 160 μM DMSO added to media for the LND and α-Cinn treatments, respectively. 2-NBDG-labeled controls without DMSO were tested simultaneously and compared to DMSO-treated controls (not shown), and DMSO was shown to increase overall 2-NBDG fluorescence which reflects an increase in cell membrane permeability. Therefore, the vehicle controls treated with DMSO are shown in the Results (Fig. 4) to control for the effect of DMSO on 2-NBDG uptake in the LND and α-Cinn experiments.

Finally, MCF7, an ER+, and MDA-MB-435, an ER−, cell lines were treated with tam. Tam is a commonly used endocrine therapy that specifically targets ER [14] and is, therefore, a good candidate to demonstrate the applicability of 2-NBDG to breast cancer. Tam has been shown to decrease glycolysis [19, 24, 25] and inhibit GLUT 1 in vitro in tam-sensitive cells [19]. Previous studies have also shown a decrease in glycolysis after tam treatment by imaging FDG uptake [26, 27]. Uptake of 2-NBDG significantly decreased after treatment in MCF7 cells, but did not change in the MDA-MB-435 cell line. No response in the MDA-MB-435 cells showed the ability of 2-NBDG to monitor therapy response. An independent western blot analysis showed that GLUT 1 is important in the uptake of 2-NBDG in breast cancer.

The cellular origin of the MDA-MB-435 cell line has recently been questioned. Our group has previously reported similar uptake of aminolevulinic acid in MDA-MB-435, implying the cell line is similar to breast [15]. Although, it has previously been shown that the MDA-MB-435 has a gene expression profile consistent with M14 melanoma cells, recently Chambers [28] has argued that the MDA-MB-435 cell line is indeed of breast cancer origin. The argument stated that MDA-MB-435 originated from a female and the original M14 melanoma line was reported to be derived from a male patient [28]. The current M14 melanoma line stock does not contain a Y chromosome, which indicates that the M14 was most likely compromised [28]. In spite of the controversy surrounding the origin of the MDA-MB-435 cell line, the results from this study demonstrate concordance between MDA-MB-435 and the other breast cancer cell lines studied in terms of its uptake of 2-NBDG.

(2-(*N*-(7-nitrobenz-2-oxa-1,3-diazol-4-yl)amino)-2-deoxyglucose) uptake is a simple method to monitor changes in glycolysis and effectiveness of therapy. 2-NBDG can be further implemented in animal models to monitor the effects of drugs that affect glycolysis over time in vivo. Sheth et al. have successfully used an RFP murine dorsal window chamber model to show the overlap in 2-NBDG

uptake and RFP-labeled cancer cells [12]. Dorsal window chambers with 2-NBDG imaging would allow for longitudinal studies to examine effectiveness of therapies that perturb glycolysis. Other possibilities for pre-clinical monitoring of in vivo therapy could be to use spectroscopy or spectral imaging to monitor changes in 2-NBDG uptake in solid tumors. By utilizing the 2-NBDG molecule in conjunction with confocal, wide-field, or spectroscopy systems, glucose monitoring cost can be greatly reduced over other options such as microPET.

Acknowledgments The authors would like to acknowledge the support of the NIH Imaging Training Grant and DOD grant W81XWH-05-1-0363. Also, the Seewaldt lab has been especially helpful and is greatly appreciated for training SM in the use of molecular assays and for providing access to appropriate laboratory equipment.

References

1. Biersack HJ, Bender H, Palmedo H (2004) FDG-PET in monitoring therapy of breast cancer. Eur J Nucl Med Mol Imaging 31(Suppl 1):S112–S117
2. Nitin N, Carlson AL, Muldoon T, El-Naggar AK, Gillenwater A et al (2009) Molecular imaging of glucose uptake in oral neoplasia following topical application of fluorescently labeled deoxy-glucose. Int J Cancer 124:2634–2642
3. O'Neil RG, Wu L, Mullani N (2005) Uptake of a fluorescent deoxyglucose analog (2-NBDG) in tumor cells. Mol Imaging Biol 7:388–392
4. Livshits L, Caduff A, Talary MS, Lutz HU, Hayashi Y et al (2009) The role of GLUT1 in the sugar-induced dielectric response of human erythrocytes. J Phys Chem B 113:2212–2220
5. Meira DD, Marinho-Carvalho MM, Teixeira CA, Veiga VF, Da Poian AT et al (2005) Clotrimazole decreases human breast cancer cells viability through alterations in cytoskeleton-associated glycolytic enzymes. Mol Genet Metab 84:354–362
6. He Q, Xu RZ, Shkarin P, Pizzorno G, Lee-French CH et al (2003) Magnetic resonance spectroscopic imaging of tumor metabolic markers for cancer diagnosis, metabolic phenotyping, and characterization of tumor microenvironment. Dis Markers 19:69–94
7. Furman E, Rushkin E, Margalit R, Bendel P, Degani H (1992) Tamoxifen induced changes in MCF7 human breast cancer: in vitro and in vivo studies using nuclear magnetic resonance spectroscopy and imaging. J Steroid Biochem Mol Biol 43:189–195
8. Mestres P, Morguet A, Schmidt W, Kob A, Thedinga E (2006) A new method to assess drug sensitivity on breast tumor acute slices preparation. Ann N Y Acad Sci 1091:460–469
9. Ramanujan VK, Herman BA (2008) Nonlinear scaling analysis of glucose metabolism in normal and cancer cells. J Biomed Opt 13:031219
10. Yoshioka K, Saito M, Oh KB, Nemoto Y, Matsuoka H et al (1996) Intracellular fate of 2-NBDG, a fluorescent probe for glucose uptake activity, in *Escherichia coli* cells. Biosci Biotechnol Biochem 60:1899–1901
11. Bos R, van Der Hoeven JJ, van Der Wall E, van Der Groep P, van Diest PJ et al (2002) Biologic correlates of (18)fluorodeoxyglucose uptake in human breast cancer measured by positron emission tomography. J Clin Oncol 20:379–387
12. Sheth RA, Josephson L, Mahmood U (2009) Evaluation and clinically relevant applications of a fluorescent imaging analog to fluorodeoxyglucose positron emission tomography. J Biomed Opt 14:064014
13. Levi J, Cheng Z, Gheysens O, Patel M, Chan CT et al (2007) Fluorescent fructose derivatives for imaging breast cancer cells. Bioconjug Chem 18:628–634
14. Dietze EC, Troch MM, Bean GR, Heffner JB, Bowie ML et al (2004) Tamoxifen and tamoxifen ethyl bromide induce apoptosis in acutely damaged mammary epithelial cells through modulation of AKT activity. Oncogene 23:3851–3862
15. Millon SR, Ostrander JH, Yazdanfar S, Brown JQ, Bender JE et al (2010) Preferential accumulation of 5-aminolevulinic acid-induced protoporphyrin IX in breast cancer: a comprehensive study on six breast cell lines with varying phenotypes. J Biomed Opt 15:018002
16. Erlichman JS, Hewitt A, Damon TL, Hart M, Kurascz J et al (2008) Inhibition of monocarboxylate transporter 2 in the retrotrapezoid nucleus in rats: a test of the astrocyte-neuron lactate-shuttle hypothesis. J Neurosci 28:4888–4896
17. Floridi A, Paggi MG, D'Atri S, De Martino C, Marcante ML et al (1981) Effect of lonidamine on the energy metabolism of Ehrlich ascites tumor cells. Cancer Res 41:4661–4666
18. Pincheira R, Chen Q, Zhang JT (2001) Identification of a 170-kDa protein over-expressed in lung cancers. Br J Cancer 84:1520–1527
19. Rivenzon-Segal D, Boldin-Adamsky S, Seger D, Seger R, Degani H (2003) Glycolysis and glucose transporter 1 as markers of response to hormonal therapy in breast cancer. Int J Cancer 107:177–182
20. Pelicano H, Martin DS, Xu RH, Huang P (2006) Glycolysis inhibition for anticancer treatment. Oncogene 25:4633–4646
21. Brown RS, Goodman TM, Zasadny KR, Greenson JK, Wahl RL (2002) Expression of hexokinase II and Glut-1 in untreated human breast cancer. Nucl Med Biol 29:443–453
22. Di Cosimo S, Ferretti G, Papaldo P, Carlini P, Fabi A et al (2003) Lonidamine: efficacy and safety in clinical trials for the treatment of solid tumors. Drugs Today (Barc) 39:157–174
23. Sonveaux P, Vegran F, Schroeder T, Wergin MC, Verrax J et al (2008) Targeting lactate-fueled respiration selectively kills hypoxic tumor cells in mice. J Clin Invest 118:3930–3942
24. Rivenzon-Segal D, Margalit R, Degani H (2002) Glycolysis as a metabolic marker in orthotopic breast cancer, monitored by in vivo (13)C MRS. Am J Physiol Endocrinol Metab 283:E623–E630
25. Perumal SS, Shanthi P, Sachdanandam P (2005) Therapeutic effect of tamoxifen and energy-modulating vitamins on carbohydrate-metabolizing enzymes in breast cancer. Cancer Chemother Pharmacol 56:105–114
26. Monazzam A, Josephsson R, Blomqvist C, Carlsson J, Langstrom B et al (2007) Application of the multicellular tumour spheroid model to screen PET tracers for analysis of early response of chemotherapy in breast cancer. Breast Cancer Res 9:R45
27. Monazzam A, Razifar P, Simonsson M, Qvarnstrom F, Josephsson R et al (2006) Multicellular tumour spheroid as a model for evaluation of [18F]FDG as biomarker for breast cancer treatment monitoring. Cancer Cell Int 6:6
28. Chambers AF (2009) MDA-MB-435 and M14 cell lines: identical but not M14 melanoma? Cancer Res 69:5292–5293

Published OnlineFirst May 11, 2010; DOI:10.1158/0008-5472.CAN-09-2572

Tumor and Stem Cell Biology

Cancer Research

Optical Redox Ratio Differentiates Breast Cancer Cell Lines Based on Estrogen Receptor Status

Julie Hanson Ostrander[1], Christine M. McMahon[2], Siya Lem[1], Stacy R. Millon[2], J. Quincy Brown[2], Victoria L. Seewaldt[1], and Nimmi Ramanujam[2]

Abstract

Autofluorescence spectroscopy is a powerful imaging technique that exploits endogenous fluorophores. The endogenous fluorophores NADH and flavin adenine dinucleotide (FAD) are two of the principal electron donors and acceptors in cellular metabolism, respectively. The optical oxidation-reduction (redox) ratio is a measure of cellular metabolism and can be determined by the ratio of NADH/FAD. We hypothesized that there would be a significant difference in the optical redox ratio of normal mammary epithelial cells compared with breast tumor cell lines and that estrogen receptor (ER)–positive cells would have a higher redox ratio than ER-negative cells. To test our hypothesis, the optical redox ratio was determined by collecting the fluorescence emission for NADH and FAD via confocal microscopy. We observed a statistically significant increase in the optical redox ratio of cancer compared with normal cell lines ($P < 0.05$). Additionally, we observed a statistically significant increase in the optical redox ratio of ER(+) breast cancer cell lines. The level of *ESR1* expression, determined by real-time PCR, directly correlated with the optical redox ratio (Pearson's correlation coefficient = 0.8122, $P = 0.0024$). Furthermore, treatment with tamoxifen and ICI 182,870 statistically decreased the optical redox ratio of only ER(+) breast cancer cell lines. The results of this study raise the important possibility that fluorescence spectroscopy can be used to identify subtypes of breast cancer based on receptor status, monitor response to therapy, or potentially predict response to therapy. This source of optical contrast could be a potentially useful tool for drug screening in preclinical models. *Cancer Res; 70(11); 4759–66. ©2010 AACR.*

Introduction

Fluorescence microscopy is a useful tool to characterize the metabolic properties of normal and cancerous cells and tissue (1, 2). The primary oxidation-reduction (redox) reactions in cells to generate energy in the form of ATP are the conversion of NAD^+ to its reduced form NAD(P)H (henceforth referred to as NADH) and the oxidation of flavin adenine dinucleotide (FAD) to $FADH_2$, a process known as oxidative phosphorylation. Both NADH and FAD are autofluorescent and have distinct excitation and emission maxima. The optical redox ratio can be determined by calculating the ratio of the measured fluorescence intensities of NADH and FAD (NADH/FAD; ref. 3).

Alterations in cellular metabolism are an important hallmark of carcinogenesis (4). Cancer cell metabolism is often shifted from oxidative phosphorylation to aerobic glycolysis as the primary generator of cellular ATP. Although the exact mechanisms for the switch to aerobic glycolysis and altered cellular metabolism are variable and complex (4, 5), it presents clear advantages for tumor growth. These advantages include resistance to fluctuations in the local oxygen concentration (6) and alterations in the tumor microenvironment that support tumor cell migration and invasion (7, 8). This shift, which gives rise to enhanced production of lactate in the presence of high oxygen, has long been known as the "Warburg effect" (9). In aerobic glycolysis, glucose is metabolized into two pyruvate molecules, which are then converted into lactate. This results in the production of two molecules of ATP and two NADH. During oxidative phosphorylation, one molecule of glucose is converted to carbon dioxide and water, resulting in the production of 30 to 36 ATP molecules and the oxidation of 10 NADH molecules to NAD^+. Thus, the switch from oxidative phosphorylation to aerobic glycolysis results in a net increase in NADH.

Estrogens and estrogen receptors (ER) have been shown to play a role in numerous aspects of cellular metabolism in a number of organ systems, including the liver, pancreas, brain, muscle, and breast (10, 11). Estrogens/ER have been shown to increase glucose transport and glycolysis (12–15). For example, estrogen exposure has been shown to increase the expression of a number of glucose transporter (GLUT) proteins (12, 15, 16). Estrogen (but not the ER antagonist tamoxifen) increased glucose uptake and lactate production in MCF-7 xenografts as measured by C^{13} nuclear magnetic resonance imaging (13). Additionally, estrogens/ER regulate

Authors' Affiliations: [1]Department of Medicine, Division of Medical Oncology, Duke University Medical Center and [2]Department of Biomedical Engineering, Fitzpatrick Institute for Photonics, Duke University, Durham, North Carolina

Corresponding Author: Julie H. Ostrander, Duke University Medical Center, DUMC, Box 2628, MSRB 215, Durham, NC 27710. Phone: 919-668-2457; Fax: 919-668-2458; E-mail: julie.ostrander@duke.edu.

doi: 10.1158/0008-5472.CAN-09-2572

Published OnlineFirst May 11, 2010; DOI:10.1158/0008-5472.CAN-09-2572

gene expression of proteins involved in the citric acid cycle and oxidative phosphorylation (10). Although not specifically studied in the breast, estrogen/ER have been shown to regulate citrate synthase, aconitase, and isocitrate dehydrogenase (17–20). Notably, isocitrate dehydrogense activity results in the reduction of NAD^+ to NADH, which is expected to cause an increase in the optical redox ratio. Furthermore, ER has been shown to localize to the mitochondria in a variety of cell types (10), and it has been proposed that mitochondrial localization of ER is important for the transcriptional regulation of numerous mitochondrial DNA–encoded genes.

Previous studies have shown that the optical redox ratio is statistically different between cancer and normal epithelial cells, with cancer cells exhibiting higher redox ratios (2, 3, 21, 22). For example, in a study comparing normal keratinocytes to human papillomavirus (HPV)–transformed cells, the authors found that HPV-transformed cells had a higher overall intensity of NADH and a lower overall intensity of FAD, which resulted in a statistically significant difference in the optical redox ratio (22). However, the optical redox ratio of NADH to FAD has not been quantified for different biological subtypes of breast cancer, nor has its relationship to breast cancer ER status been assessed.

Based on previously published reports in the literature, our primary hypotheses tested in this study were that the optical redox ratio can differentiate between malignant and nonmalignant breast cells and between ER(+) and ER(−) breast cancer cell lines. A secondary hypothesis is that the optical redox ratio can specifically monitor response to antiestrogen therapies. To test our hypotheses, we determined the optical redox ratio using a confocal microscopy approach. NADH and FAD intensities were acquired from a panel of normal mammary epithelial and breast cancer cell lines following excitation at 351 and 488 nm, respectively. The optical redox ratio differentiated normal mammary epithelial cells from breast cancer cells and also stratified breast cancer cell lines based on ER expression, which was associated with an increased optical redox ratio. Further, treatment of ER(+) breast cancer cell lines with antiestrogens resulted in a decrease in the optical redox ratio. This effect was not observed in ER(−) cell lines.

ER has proved to be a successful target of antitumor therapy in ER(+) breast tumors. However, resistance to antiestrogen therapies is a serious clinical problem for the treatment of breast cancer. Whereas ER expression is a good predictor of response to antiestrogen therapies, not all ER(+) tumors respond to therapy and some develop resistance after initially responding to therapy. Therefore, the optical redox ratio may serve as an important biomarker to differentially identify ER(+) breast cancers and monitor response to antiestrogen therapy, with applications in drug discovery and screening as well as clinical assessment of response to antiestrogen therapies.

Materials and Methods

Cell culture and reagents

MCF-10A, MDA-231, MDA-435, MDA-468, BT-20, BT-474, MDA-361, MCF-7, T47D, and ZR-75-1 cells were obtained from either the American Type Culture Collection or the Duke Cell Culture Facility. Primary human mammary epithelial cells (HMEC) were obtained from Lonza and transduced with a retrovirus encoding human telomerase catalytic subunit (hTERT). Cells that incorporated hTERT were selected with puromycin and resistant cells were pooled and used for subsequent experiments. All cell lines except MCF-10A and HMEC were cultured in minimal essential medium α (Invitrogen) supplemented with 5% fetal bovine serum, 10 mmol/L HEPES (Invitrogen), 1× nonessential amino acids (Invitrogen), 1× sodium pyruvate (Invitrogen), 1 μg/mL insulin (Invitrogen), 1 μg/mL hydrocortisone (Sigma Aldrich), and 10 ng/mL epidermal growth factor (EGF; Sigma Aldrich). MCF-10A and HMEC were cultured in MEBM (Lonza) containing insulin, EGF, hydrocortisone, and bovine pituitary extract. All cell lines were tested for *Mycoplasma* contamination at the time of purchase and all experiments were done within 6 months of purchasing cell lines.

Confocal microscopy

For all experiments testing the optical redox ratio, cells were plated at 1×10^5 per 35-mm glass-bottomed dish (MatTek Corporation). For the panel of normal mammary epithelial cells and breast cancer cell lines, cell images were obtained approximately 48 hours later on a Zeiss LSM 410 confocal microscope (Duke University Light Microscopy Core Facility). NADH intensity images were obtained by excitation at 351 nm with a Coherent Enterprise II UV laser and the emission collected with a 400-nm LP filter. FAD intensity images were obtained by excitation at 488 nm with an Omnichrome KrAr laser and the emission collected with a 505-nm LP filter. Settings for NADH were gain = 9,611, offset = 411, and for FAD, gain = 9,555, offset = 490; the pinhole was set at 1,488 μm for both NADH and FAD. The pinhole, gain, and offset remained the same for every experiment. A model cell line, MCF-10A, was imaged during each experiment to confirm that the laser power and instrument settings were comparable from day to day (internal control). For cells treated with the antiestrogens tamoxifen (Tam) or ICI 182,780 (ICI; Sigma Aldrich), cells were plated as described above, and then approximately 24 hours later, cells were treated with 2 μmol/L Tam, 100 nmol/L ICI, or vehicle control (ethanol or DMSO). Images were acquired approximately 48 hours following treatment. Each cell line was imaged on at least 2 separate days. For each imaging session, there were two plates of each cell line and two fields of view (320 μm × 320 μm) for both NADH and FAD. All images were acquired with a 40× oil objective. Each image was line averaged 16 times, and image acquisition took approximately 16 seconds. Following data collection, the NADH/FAD ratio (a measure of the reduction-oxidation ratio) was calculated for every cell in each image. For each acquired NADH and FAD image, ImageJ software (NIH, ref. 23) was used to obtain the integrated intensity of NADH and FAD for each cell in the image after the background fluorescence was subtracted. NADH values were divided by the FAD value for each cell in an image and the average NADH/FAD was calculated for the entire image ($n = 1$). All images ($n \geq 8$) were then averaged to determine the optical redox ratio.

Published OnlineFirst May 11, 2010; DOI:10.1158/0008-5472.CAN-09-2572

Table 1. Summary of cell line data

Cell line	Normal vs cancer	ER status	Plates imaged	No. of images (*n*)
MCF-10A	Normal	–/low	18	36
HMEC	Normal	–/low	4	8
	Total normal		22	44
MDA-231	Cancer	Negative	5	10
MDA-435	Cancer	Negative	5	10
MDA-468	Cancer	Negative	4	8
BT-20	Cancer	Negative	4	8
	Total ER(–)		18	36
BT-474	Cancer	Positive	6	12
MDA-361	Cancer	Positive	6	12
MCF-7	Cancer	Positive	6	12
T47D	Cancer	Positive	4	8
ZR-75-1	Cancer	Positive	4	8
	Total ER(+)		26	52

RNA isolation, cDNA synthesis, and quantitative real-time PCR

To test for *ESR1* expression, total RNA from normal mammary epithelial cells and breast cancer cell lines (two independent cultures from each cell line) was isolated using the RNeasy Mini Kit (Qiagen) according to the manufacturer's instructions. On-column DNase digestions were done to eliminate any genomic DNA contamination using the RNase-Free DNase Set (Qiagen). Total RNA quantity and quality were determined using the NanoDrop ND-1,000 full-spectrum UV/Vis spectrophotometer V3.1.2. All of the RNA that was used in this study had a 260:280 ratio between 2.1 and 2.2. RNA integrity was analyzed using the Experion RNA HighSens Analysis Kit (Bio-Rad), which confirmed the

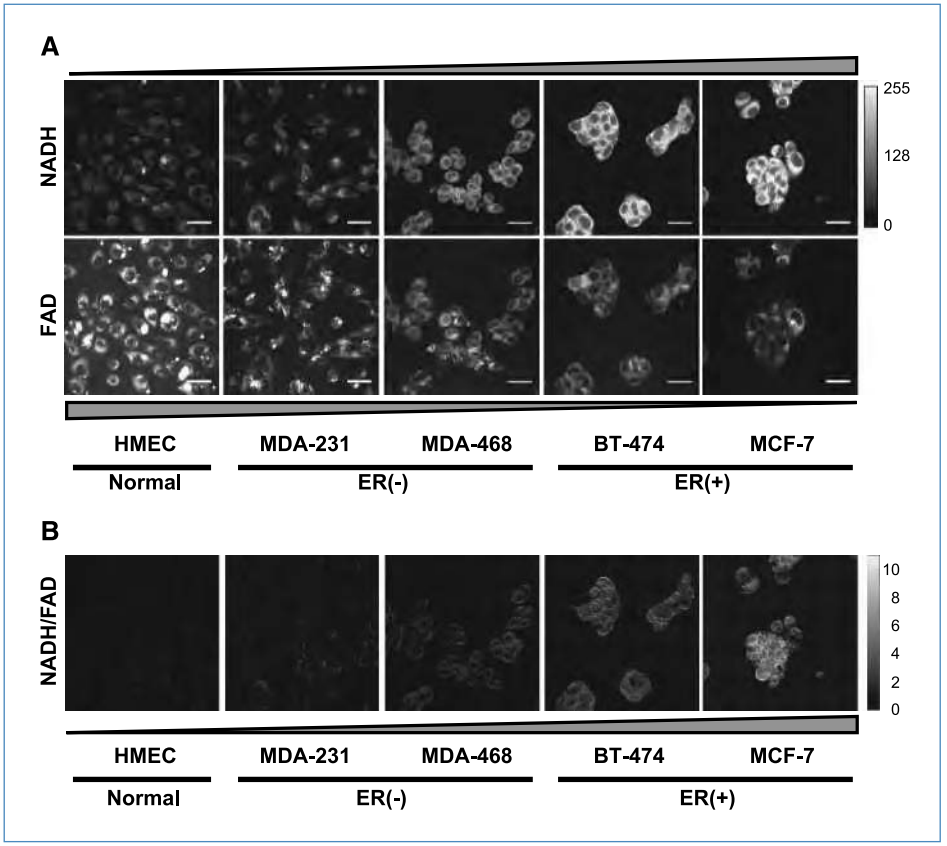

Figure 1. NADH and FAD images from breast cancer cell lines. A, representative NADH and FAD images from normal mammary epithelial cells (HMEC), ER(–) breast cancer cell lines (MDA-231 and MDA-468), and ER(+) breast cancer cell lines (BT-474 and MCF-7). Bar, 50 μm. B, redox ratio images corresponding to representative images in A, computed by dividing NADH images by FAD images pixel by pixel. The color scale (shown at the right of the figure) was optimized for MCF-7 cells and was kept constant for all images to allow direct visual comparison of redox ratio images across cell lines.

Published OnlineFirst May 11, 2010; DOI:10.1158/0008-5472.CAN-09-2572

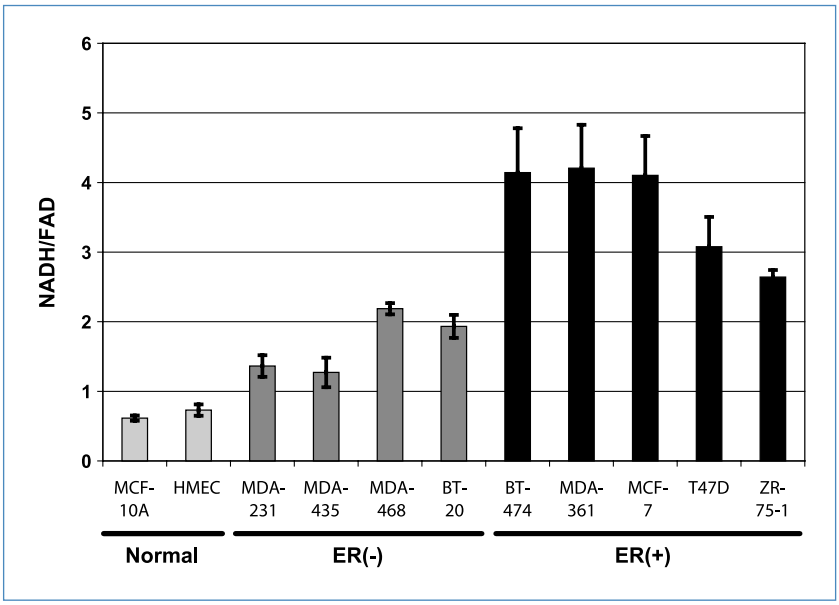

Figure 2. Optical redox ratio differentiates breast cancer cell lines. Optical redox ratio (NADH/FAD) of individual cell lines from a panel of normal mammary epithelial and breast cancer cell lines. Cell lines are grouped by normal mammary epithelial cells (light gray columns), ER(–) breast cancer cell lines (medium gray columns), and ER(+) breast cancer cell lines (black bars). Bars, SE.

presence of intact 18S and 28S rRNA. First-strand cDNA was synthesized from total RNA using the SuperScript III First-Strand Synthesis System for reverse transcription-PCR (RT-PCR; Invitrogen) according to the manufacturer's protocol.

cDNA was amplified using the QuantiTect SYBR Green PCR master mix (Qiagen) on a Bio-Rad iCycler MyiQ Single-Color Real-time PCR Detection System. *ESR1* amplification conditions were 95°C for 15 minutes, followed by 40 cycles of 95°C for 30 seconds, 58°C for 30 seconds, and 72°C for 30 seconds. 18S amplification conditions were identical except for an annealing temperature of 53°C. *ESR1* primer sequences were generated using VectorNTI software (Invitrogen): *ESR1*-F, 5′-CAGCTGTCGCCTTTCCTGCA-3′; *ESR1*-R, 5′-CACCCTGGCGTCGATTATCT-3′; 18S primers were purchased from Qiagen (QT00199367). Temperature gradients were performed to ensure that the annealing temperature for each gene was optimal. Melting curve analysis was done at the end of the PCR reaction to confirm that only one amplified product was detected. PCR amplification data were analyzed with the MyiQ Optical System Software version 1.0 (Bio-Rad). The baseline cycles and threshold were automatically calculated by the software. Because the standards were defined for each of the experimental runs, the software adjusted the threshold to attain the highest possible correlation coefficient value for the PCR standard curve. Quantitative RT-PCR was done at least twice on each cDNA from two independent RNA samples from each cell line.

Cell cycle analysis

To confirm that Tam treatment of MCF-7 cells resulted in cell cycle arrest and/or apoptosis, MCF-7 cells were plated at 2.5×10^5 per well in a six-well plate. Twenty-four hours after plating cells, triplicate wells were treated in with 2 μmol/L Tam or vehicle control for 48 hours. Cells were collected following trypsinization, washed twice with 1× PBS, and then fixed in 75% ethanol overnight. Before staining, ethanol-fixed cells were washed twice with 1× PBS. Samples were then incubated in fluorescence-activated cell sorting (FACS) staining buffer containing 1× PBS, 1 mg/mL RNase A, 0.5 μmol/L EDTA, 0.1% Triton X-100, and 100 μg/mL propidium iodide before FACS cell cycle analysis. Each experiment was repeated at least twice.

Results

Optical redox ratio differentiates breast cancer from normal cell lines

A number of previous reports suggested that the optical redox ratio (NADH/FAD) could be used to differentiate breast cancer cell lines from normal mammary epithelial cells (24, 25). To further test this hypothesis, we examined a panel of nine breast cancer cell lines and two cell line models of normal mammary epithelial cells. As described in Materials and Methods, each cell line was imaged on at least 2 separate days, two plates per cell line and two images per plate, for a minimum $n = 8$ (Table 1). MCF-10A cells, a model of normal mammary epithelial cells, were imaged each day and had a very consistent redox ratio with a small SE. Qualitatively, NADH intensity was lower and FAD intensity was higher in normal mammary epithelial cells compared with ER(–) and ER(+) breast cancer cell lines. As shown in Fig. 1A, the NADH intensity dramatically increased in ER(+) BT-474 and MCF-7 cells compared with HMEC, MDA-231, and MDA-468 cells, and FAD intensity decreased in MDA-231, MDA-468, BT-474, and MCF-7 cells compared with HMEC. Furthermore, when the NADH images were divided pixel by pixel by the FAD images, there was a dramatic increase in the NADH/FAD signal in ER(+) BT-474 and MCF-7

Published OnlineFirst May 11, 2010; DOI:10.1158/0008-5472.CAN-09-2572

cells compared with HMEC, MDA-231, and MDA-468 cells (Fig. 1B).

Following ImageJ analysis, all data for each cell line were averaged, and the results are shown in Fig. 2A. We found that the optical redox ratios of MCF-10A and HMEC lines, models of normal mammary epithelial cells, were not statistically different from each other (Student's t test, $P > 0.05$), but both MCF10A and HMEC lines had statistically different optical redox ratios when compared individually to all cancer cell lines (Student's test, $P < 0.05$). Additionally, all of the ER(+) cells had higher optical redox ratios relative to all of the ER (−) breast cancer cell lines. A Tukey-Kramer test was done to account for multiple comparisons and unequal group sizes and indicated that ER(−) and ER(+) cell lines were significantly different when data were grouped as normal mammary epithelial cells, ER(−), or ER(+).

Optical redox ratio correlates with *ESR1* expression

The results from the data presented in Figs. 1 and 2 suggest that the optical redox ratio is associated with ER expression in the breast cancer cell lines. Therefore, the ER mRNA (*ESR1*) expression levels were tested by quantitative RT-PCR to determine the association between *ESR1* expression and the optical redox ratio. Total RNA was harvested from each cell line and cDNA was prepared. Quantitative RT-PCR was then performed with primers specific to *ESR1* and *18S*. All *ESR1* data were normalized to *18S*. As shown in Fig. 3A, very low expression of *ESR1* was observed in both normal mammary epithelial cell lines and all four breast cancer cell lines previously reported to be ER(−), whereas all five breast cancer cell lines previously reported as ER(+) expressed significant amounts of *ESR1*. Interestingly, we observed low *ESR1* expression in MDA-468 and BT-20 breast cancer cell lines. These two ER(−) breast cancer cell lines had statistically significant higher redox ratios than the other two ER(−) breast cancer cell lines (MDA-231 and MDA-435; Student's t test, $P < 0.05$). To determine if *ESR1* expression positively correlated with the optical redox ratio, a Pearson's correlation test was performed. We found that *ESR1* expression and the optical redox ratio were positively correlated (Pearson's correlation coefficient = 0.8122, $P = 0.0024$), further suggesting that ER expression has an effect on the optical redox ratio.

Antiestrogens modulate the optical redox ratio

Because ER expression positively correlated with the optical redox ratio, the next logical step was to test the effects of the antiestrogens Tam and ICI on the optical redox ratio. First, the effects of Tam treatment were tested by cell cycle analysis. Tam (2 μmol/L) or vehicle control was added to the normal growth medium of triplicate cultures of MCF-7 for 48 hours. MCF-7 cells were then trypsinized and fixed in 75% ethanol overnight. Samples were then stained with propidium iodide and analyzed by flow cytometry for cell cycle distribution. After 48 hours of Tam treatment, there was a statistically significant increase in MCF-7 cells with sub-G_1 content of DNA (3.6% to 7.0%; $P < 0.0001$), indicative of apoptosis, an increase in cells in the G_1 phase of the cell cycle (53% to 64%; $P = 0.0007$), and a decrease in cells in S-phase and G_2-M (S-phase: 25% to 17%, $P = 0.0007$; G_2-M: 19% to 13%, $P = 0.0017$) as shown in Fig. 4A. The cell cycle analysis indicated that 2 μmol/L Tam has a significant effect on the proliferation and cell cycle distribution of MCF-7 cells. Similar results were also obtained for MCF-7 cells treated with 100 nmol/L ICI (data not shown).

To test for Tam-induced changes in the optical redox ratio, ER(+) MCF-7 and T47D cells were treated for 48 hours with 2 μmol/L Tam or vehicle control, and NADH and FAD autofluorescence were measured as described above. Tam treatment resulted in a statistically significant decrease in the optical redox ratio in both MCF-7 and T47D breast cancer

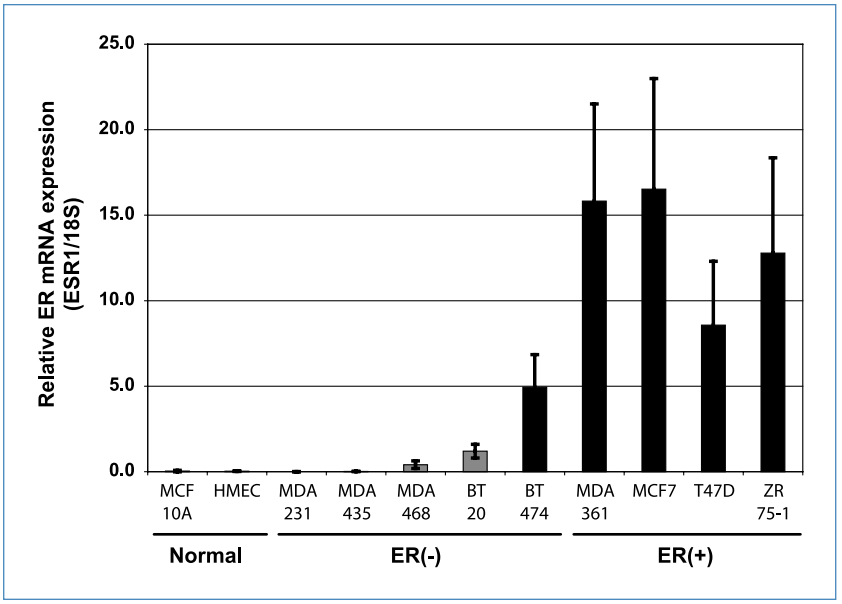

Figure 3. Optical redox ratio correlates with ESR1 expression. Quantitative RT-PCR data from normal mammary epithelial and breast cancer cell lines. All ESR1 expression data were normalized to *18S* levels in the same sample. Data presented are the average of four independent quantitative RT-PCR reactions from two separate RNA extractions for each cell line. Bars, SD.

Published OnlineFirst May 11, 2010; DOI:10.1158/0008-5472.CAN-09-2572

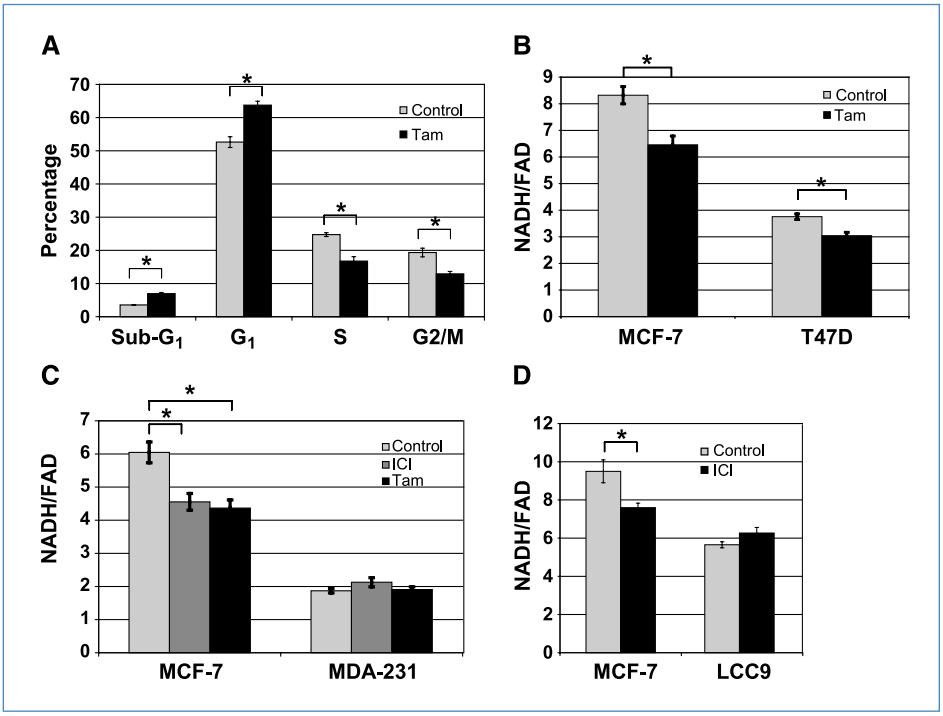

Figure 4. Antiestrogens modulate the optical redox ratio. A, flow cytometry cell cycle analysis from propidium iodide–stained vehicle control (EtOH)– and Tam-treated (48 h) MCF-7 cells. Bars, SD; *, $P < 0.05$ (Student's t test). B, optical redox ratio from ER(+) MCF-7 and T47D cells treated with vehicle control or 2 μmol/L Tam for 48 h. C, optical redox ratio was measured from vehicle control– (light gray columns), ICI- (medium gray columns), and Tam-treated (black columns) ER(+) MCF-7 and ER(–) MDA-231 cells. D, optical redox ratio was measured from parental MCF-7 cells and MCF-7–derived LCC9 cells (Tam-resistant, ICI-resistant) treated with 100 nmol/L ICI for 48 h. B to D, bars, SE; *, $P < 0.05$ (Student's t test).

cell lines (Student's t test, $P < 0.05$; Fig. 4B). Next, the effects of Tam and ICI on ER(+) MCF-7 and ER(–) MDA-231 cells were tested. The underlying hypothesis was that if the optical redox ratio is dependent on ER signaling, then the optical redox ratio of MCF-7 cells treated with Tam or ICI would decrease. However, the optical redox ratio of ER(–) MDA-231 cells would remain unchanged. Indeed, both Tam and ICI had a statistically significant effect on the optical redox ratio of MCF-7 cells (Student's t test, $P < 0.05$), but not MDA-231 breast cancer cells, as shown in Fig. 4C.

An MCF-7 variant cell line, LCC9, was also acquired from Robert Clarke at Georgetown University (26). The LCC9 cells are ER(+) but resistant to Tam and ICI. Parental MCF-7 and LCC9 cells were treated with either vehicle control or 100 nmol/L ICI for 48 hours. ICI-treated parental MCF-7 cells had a statistically significant lower optical redox ratio compared with vehicle control–treated MCF-7 cells (Student's t test, $P < 0.05$), whereas the optical redox ratio of LCC9 cells was not significantly affected by ICI treatment (Fig. 4D). Together, the data in Fig. 4 suggest that ER antagonists reduce the optical redox ratio in ER(+) breast cancer cells, but not in ER(–) or antiestrogen-resistant cell lines.

Discussion

Our study shows that the optical redox ratio (*a*) differentiates normal mammary epithelial cells from a panel of breast cancer cell lines (Fig. 2), (*b*) positively correlates with ER expression (Fig. 3), and (*c*) can be used to monitor response to antiestrogen therapy (Fig. 4).

This is the first study to examine the optical redox ratio in a panel of cell lines that includes both normal mammary epithelial cells and ER(+) and ER(–) breast cancer cell lines. Similar to our findings (Fig. 1A), a number of studies have found that NADH intensity is higher in cancer cells and high-grade dysplasia compared with normal tissue or cell lines (24, 25, 27). In a study of 35 suspected cervical lesions and 7 cases of Barrett's esophagus, higher NADH fluorescence was observed in high-grade dysplastic lesions compared with nondysplastic tissue (27). Another study, which compared one breast cancer cell line and one normal mammary epithelial cell line, found that NADH intensity was 1.8-fold higher in the breast cancer cell line (25). Interestingly, a third study found that whereas breast cancer tissue had elevated NADH compared with normal tissue, the opposite was true for oral cancers (24), suggesting that transformation-induced changes in the optical redox ratio may be specific to organ site.

Contrary to the results presented here, in a previous study by our group, NADH and FAD intensities were examined independently in MCF-10A, T47D, MDA-231, and in control and R-Ras transformed cell lines (28). This study used fluorescence spectroscopy of cell suspensions, and a statistically significant difference in NADH or FAD intensity between malignant and nonmalignant cells was not observed. One explanation for the differences in findings between our current monolayer and previous cell suspension studies is likely due to the fact that fluorescence intensity of cells in suspension is prone to random error not present in monolayer studies. Specifically, the effects of scattering from cell suspended in media can randomly attenuate or increase the fluorescence. Further, whereas NADH and FAD intensity values

Published OnlineFirst May 11, 2010; DOI:10.1158/0008-5472.CAN-09-2572

provide a measure of the metabolic state, the ratio of NADH and FAD is a more robust measurement in that it provides an internal control for cell density and instrument throughput variations.

The effect of ER expression on the optical redox ratio is not surprising. As stated above, estrogens and ERs have been shown to play a role in numerous aspects of cellular metabolism (10). The results presented here further indicate the importance of estrogen/ER in cancer cell metabolism. Based on previous reports (12–15), the dramatic increase in the optical redox ratio is likely due to an increase in glucose transport and aerobic glycolysis, which results in an increase in NADH. Considering the plethora of metabolic pathways estrogens/ERs have been shown to participate in, this is likely not the whole story. Future cell culture studies may provide insight into the molecular mechanisms underlying estrogen/ER–induced effects on the optical redox ratio.

Although our study is the first to demonstrate that the optical redox ratio can be used to monitor response to antiestrogen therapy, our results are consistent with a previous study which showed that the optical redox ratio is modulated in response to the chemoprevention agent *N*-4-(hydroxyphenol)-retinamide (4HPR) in bladder and ovarian cancer cell lines (21). In the study by Kirkpatrick and colleagues, fluorescence spectroscopy was used to measure NADH and FAD intensities. Samples were excited from 270 to 700 nm to generate excitation-emission matrices from cells in suspension. NADH intensity was calculated from the excitation at 350 nm with emission wavelengths 445 to 455 nm. FAD intensity was calculated from the excitation at 450 nm with emission wavelengths 530 to 540 nm. This study, which measured the optical redox ratio as FAD/(FAD+NADH), showed a dose-dependent increase in the optical redox ratio of cells treated with 4HPR, which correlated with a significant decrease in NADH intensity. Furthermore, cell lines that exhibited a greater response to 4HPR, as assessed by cell cycle analysis, also showed an increase in the optical redox ratio. Together, our studies suggest that the optical redox ratio is a good biomarker to differentially identify ER(+) breast cancer cells and to monitor response to antiestrogen therapies. Additional studies in cell lines will allow us to further test the mechanism of ER-induced effects on the optical redox ratio. A better understanding of how ER regulates cellular metabolism may lead to additional targets for more effective therapies and for prevention of resistance to antiestrogens.

If, as our data suggest, ER has a profound effect on the optical redox ratio, our cell line data should be recapitulated in mouse models *in vivo*. We have already begun to implement fiber-optic based fluorescence spectroscopy to measure optical redox ratios in small animal models. In a recent study, we noninvasively measured hemoglobin saturation and the optical redox ratio in response to carbogen breathing in a mouse tumor model (29). Quantitative optical spectroscopy measurements of hemoglobin saturation were consistent with invasive measurements of pO_2 using an OxyLite partial oxygen pressure sensor, suggesting that noninvasive optical techniques have the potential to reliably measure changes in tumor physiology. Importantly, in individual animals there was a strong linear correlation between hemoglobin saturation and the redox ratio following the administration of carbogen, reflecting the expected relationship between redox ratio and hemoglobin saturation (oxygen demand and supply). In conclusion, optical technologies are available to measure the optical redox ratio as well as other relevant parameters, such as hemoglobin oxygenation, *in vivo*. Thus, this parameter, which has been shown to have significance in our cell study, can be translated to measurements in small animal models and ultimately in patients.

Disclosure of Potential Conflicts of Interest

No potential conflicts of interest were disclosed.

Grant Support

Department of Defense Breast Cancer Research Program Multidisciplinary Postdoctoral Award (J.H. Ostrander) and an Era of Hope Scholar Award (N. Ramanujam).

The costs of publication of this article were defrayed in part by the payment of page charges. This article must therefore be hereby marked *advertisement* in accordance with 18 U.S.C. Section 1734 solely to indicate this fact.

Received 07/09/2009; revised 12/10/2009; accepted 03/24/2010; published OnlineFirst 05/11/2010.

References

1. Breslin TM, Xu F, Palmer GM, Zhu C, Gilchrist KW, Ramanujam N. Autofluorescence and diffuse reflectance properties of malignant and benign breast tissues. Ann Surg Oncol 2004;11:65–70.
2. Skala MC, Riching KM, Gendron-Fitzpatrick A, et al. *In vivo* multiphoton microscopy of NADH and FAD redox states, fluorescence lifetimes, and cellular morphology in precancerous epithelia. Proc Natl Acad Sci U S A 2007;104:19494–9.
3. Chance B, Schoener B, Oshino R, Itshak F, Nakase Y. Oxidation-reduction ratio studies of mitochondria in freeze-trapped samples. NADH and flavoprotein fluorescence signals. J Biol Chem 1979;254:4764–71.
4. Kroemer G, Pouyssegur J. Tumor cell metabolism: cancer's Achilles' heel. Cancer Cell 2008;13:472–82.
5. Brandon M, Baldi P, Wallace DC. Mitochondrial mutations in cancer. Oncogene 2006;25:4647–62.
6. Pouyssegur J, Dayan F, Mazure NM. Hypoxia signalling in cancer and approaches to enforce tumour regression. Nature 2006;441:437–43.
7. Izumi H, Torigoe T, Ishiguchi H, et al. Cellular pH regulators: potentially promising molecular targets for cancer chemotherapy. Cancer Treat Rev 2003;29:541–9.
8. Walenta S, Wetterling M, Lehrke M, et al. High lactate levels predict likelihood of metastases, tumor recurrence, and restricted patient survival in human cervical cancers. Cancer Res 2000;60:916–21.
9. Warburg O. On the origin of cancer cells. Science (New York, NY) 1956;123:309–14.
10. Chen JQ, Brown TR, Russo J. Regulation of energy metabolism pathways by estrogens and estrogenic chemicals and potential implications in obesity associated with increased exposure to endocrine disruptors. Biochim Biophys Acta 2009;1793:1128–43.
11. Duckles SP, Krause DN, Stirone C, Procaccio V. Estrogen and

Published OnlineFirst May 11, 2010; DOI:10.1158/0008-5472.CAN-09-2572

mitochondria: a new paradigm for vascular protection? Mol Interv 2006;6:26–35.
12. Cheng CM, Cohen M, Wang J, Bondy CA. Estrogen augments glucose transporter and IGF1 expression in primate cerebral cortex. FASEB J 2001;15:907–15.
13. Furman E, Rushkin E, Margalit R, Bendel P, Degani H. Tamoxifen induced changes in MCF7 human breast cancer: *in vitro* and *in vivo* studies using nuclear magnetic resonance spectroscopy and imaging. J Steroid Biochem Mol Biol 1992;43:189–95.
14. Kostanyan A, Nazaryan K. Rat brain glycolysis regulation by estradiol-17β. Biochim Biophys Acta 1992;1133:301–6.
15. Welch RD, Gorski J. Regulation of glucose transporters by estradiol in the immature rat uterus. Endocrinology 1999;140:3602–8.
16. Macheda ML, Rogers S, Best JD. Molecular and cellular regulation of glucose transporter (GLUT) proteins in cancer. J Cell Physiol 2005; 202:654–62.
17. Beckett T, Tchernof A, Toth MJ. Effect of ovariectomy and estradiol replacement on skeletal muscle enzyme activity in female rats. Metabolism 2002;51:1397–401.
18. Pastorelli R, Carpi D, Airoldi L, et al. Proteome analysis for the identification of *in vivo* estrogen-regulated proteins in bone. Proteomics 2005;5:4936–45.
19. Stirone C, Duckles SP, Krause DN, Procaccio V. Estrogen increases mitochondrial efficiency and reduces oxidative stress in cerebral blood vessels. Mol Pharmacol 2005;68:959–65.
20. Yadav RN. Isocitrate dehydrogenase activity and its regulation by estradiol in tissues of rats of various ages. Cell Biochem Function 1988; 6:197–202.
21. Kirkpatrick ND, Zou C, Brewer MA, Brands WR, Drezek RA, Utzinger U. Endogenous fluorescence spectroscopy of cell suspensions for chemopreventive drug monitoring. Photochem Photobiol 2005;81: 125–34.
22. Mujat C, Greiner C, Baldwin A, et al. Endogenous optical biomarkers of normal and human papillomavirus immortalized epithelial cells. Int J Cancer 2008;122:363–71.
23. Software IJ. [cited; Available from: http://rsb.info.nig.gov/ij].
24. Uppal A, Gupta PK. Measurement of NADH concentration in normal and malignant human tissues from breast and oral cavity. Biotechnol Appl Biochem 2003;37:45–50.
25. Yu Q, Heikal AA. Two-photon autofluorescence dynamics imaging reveals sensitivity of intracellular NADH concentration and conformation to cell physiology at the single-cell level. J Photochem Photobiol 2009;95:46–57.
26. Brunner N, Boysen B, Jirus S, et al. MCF7/LCC9: an antiestrogen-resistant MCF-7 variant in which acquired resistance to the steroidal antiestrogen ICI 182,780 confers an early cross-resistance to the nonsteroidal antiestrogen tamoxifen. Cancer Res 1997;57: 3486–93.
27. Georgakoudi I, Jacobson BC, Muller MG, et al. NAD(P)H and collagen as *in vivo* quantitative fluorescent biomarkers of epithelial precancerous changes. Cancer Res 2002;62:682–7.
28. Palmer GM, Keely PJ, Breslin TM, Ramanujam N. Autofluorescence spectroscopy of normal and malignant human breast cell lines. Photochem Photobiol 2003;78:462–9.
29. Palmer GM, Viola RJ, Schroeder T, Yarmolenko PS, Dewhirst MW, Ramanujam N. Quantitative diffuse reflectance and fluorescence spectroscopy: tool to monitor tumor physiology *in vivo*. J Biomed Optics 2009;14:024010.